Neurovirulence of avian influenza virus is dependent on the interaction of viral NP protein with host factor FMRP in the murine brain

Xuxiao Zhang[1], Juan Pu[1], Yipeng Sun[1], Yuhai Bi[2, 3], Zhimin Jiang[1], Guanlong Xu[1], Hongyu Zhang[1], Jing Cao[4], Kin-Chow Chang[5], Jinhua Liu[1]* and Honglei Sun[1]*

[1] Key Laboratory of Animal Epidemiology of the Ministry of Agriculture, College of Veterinary Medicine, China Agricultural University, Beijing 100193, China

[2] CAS Key Laboratory of Pathogenic Microbiology and Immunology, Institute of Microbiology, Chinese Academy of Sciences, Beijing, China

[3] CAS Center for Influenza Research and Early-Warning (CASCIRE), Chinese Academy of Sciences, Beijing, China

[4] Laboratory of Anatomy of Domestic Animal, College of Veterinary Medicine, China Agricultural University, Beijing 100193, China

[5] School of Veterinary Medicine and Science, University of Nottingham, Sutton Bonington Campus, Sutton Bonington, United Kingdom

* Corresponding author

Email: shlei668@163.com or ljh@cau.edu.cn

ABSTRACT

Avian influenza viruses (AIVs) are zoonotic viruses that exhibit a range infectivity and severity in the human host. Severe human cases of AIVs infection are often accompanied by neurological symptoms; however, the factors involved in the infection of the central nervous system (CNS) are not well known. In this study, we discovered that avian-like sialic acid (SA)-α2, 3 Gal receptor is highly represented in mammalian (human and mouse) brains. In the generation of a mouse-adapted neurotropic H9N2 AIV (SD16-MA virus) in BALB/c mice, we identified key adaptive mutations in its hemagglutinin (HA) and polymerase basic protein 2 (PB2) genes that conferred gain of neurotropism and neurovirulence in mice. The SD16-MA virus showed binding affinity for avian-like SA-α2, 3 Gal receptor, enhanced viral RNP polymerase activity, and increased viral protein production and transport that culminate in elevated progeny virus production and severe pathogenicity. We further established that host Fragile X Mental Retardation Protein (FMRP), a highly expressed protein in the brain that physically associates with viral nucleocapsid protein (NP) to facilitate RNP assembly and export, is an essential host factor for the neuronal replication of neurotropic AIVs (H9N2, H5N1 and H10N7 viruses). Our study identifies a mechanistic process for avian influenza virus to acquire neurovirulence to infect the murine CNS.

IMPORTANCE

Infection of the CNS is a serious complication of human cases of AIVs infection. The viral and host factors associated with neurovirulence of AIVs infection are not well understood. We identified and functionally characterized specific changes in the viral HA and PB2 genes of a mouse-adapted neurotropic avian H9N2 virus responsible for enhanced virus replication in neuronal cells and pathogenicity in mice. Just as important, we showed that host FMRP is a crucial host factor that is necessary for neurotropic AIVs (H9N2, H5N1 and H10N7 viruses) to replicate in neuronal cells. Our findings have provided insights into the pathogenesis of neurovirulence of AIV infection.

KEYWORDS: AIVs, Mouse adaptation, Neurovirulence, FMRP

INTRODUCTION

AIVs, in particular the three most prevalent subtypes of H5, H7 and H9 viruses found in poultry, pose constant threat to public health by repeatedly breaking through host barrier and infect humans (1-4). Extended epizootics and panzootics of H5N1 viruses have led to the emergence of novel H5NX reassortants, including H5N2, H5N6, and H5N8 viruses (5-7). Up to 20-Jan-2020, the H5NX virus had caused 880 human infection cases (861 cases with H5N1 and 24 cases with H5N6) at around 60% mortality (https://www.who.int/influenza/human_animal_interface/ 2020_01_20_ table_H5N1. pdf?ua=1). A novel reassortant H7N9 influenza virus, originated from chickens, emerged in humans in 2013 and had caused five sequential outbreaks in China (3, 8, 9). As of 09-Dec-2019, 1,568 H7N9 human cases were confirmed with 616 deaths (10)(10)(10)(10)(10). H9N2 viruses circulate globally and are endemic in multiple avian species (11, 12). Recent studies indicate that H9N2 influenza viruses have acquired higher binding affinity for human-like SA-α2, 6 Gal linked receptor, and increased virulence and transmissibility in mammals (13). Collectively, current AIVs in circulation are a growing public health threat.

Although respiratory disease is a hallmark of human influenza virus infection, AIVs infection can often cause neurological complications that can be fatal. A review of clinical features of human infection with avian H5N1 virus found that 31.36% (74/236) of cases reported fussiness and irritability, and 25% (59/236) of cases showed consciousness disorder (14). Previously, we demonstrated that avian H5N1 viral RNAs and antigens were detected in neuronal cells in a human infection (15). H7N9 virus has been reported to cause encephalitis in patients (16). These

observations indicate that AIVs could cause significant damage to the CNS. Little is known about host factors that are involved in the pathogenesis of neurological complication of AIVs infection.

The attachment of viral HA spikes to SA-containing receptors on the host cell surface initiates viral infection (17). Yen *et al.* (2009) found that changes in the HA receptor-binding domain alter the ability of the H5N1 virus to spread systemically in mice and are important for the viral neurotropism (18). Schrauwen *et al.* (2012) and Suguitan *et al.* (2012) identified multibasic cleavage site in the HA protein as a virulent factor in the systemic spread of H5N1 virus in ferrets (19, 20). Residue HA 328Y in H1N1 virus (A/WSN/33) and HA 325S in H5N1 virus in mice are found to contribute to the ease of cleavage of HA protein into HA1 and HA2 which permits fusion of the viral envelope with the secondary endosome (21, 22). Additionally, mutations of PB2 E627K and NA R146N in mouse adapted AIVs are shown to be neurovirulence factors through increasing polymerase activity and binding to fibrinolytic proteasomes (23, 24). There is a need for better understanding of viral and host factors, and their interactions in the pathogenesis of neuronal infection. Targeting such factors could provide novel treatment options to prevent a fatal outcome or lasting damage from the neurological effects of AIVs infection in humans.

In the present study, we found that mutations in the HA and PB2 genes of a mouse-adapted neurotropic avian H9N2 virus conferred binding affinity for the avian-like SA-α2, 3 receptor type, and enhanced virus replication leading to elevated pathogenicity and neurovirulence in mice. We further demonstrated that neurovirulence of AIVs is dependent on the interaction between viral NP protein and host FMRP.

RESULTS

Avian-like influenza virus α-2,3-linked SA receptor is dominant in human and murine brains

We compared the distribution of SA receptors of the brain between human and mouse using lectin histochemistry. Avian and human influenza viruses preferentially bind to α-2, 3-linked and α-2, 6-linked SAs, respectively (25). We found that both avian-like SA-α2, 3 Gal and human-like SA-α2, 6 Gal receptors are expressed in human and murine cerebrum tissues (Fig. 1). Avian-like SA-α2, 3 Gal receptor appeared dominant in the brain of both species (Fig. 1), which is unlike that of human upper respiratory tract where SA-a2,6 Gal receptor is more abundant (26). This distribution could facilitate preferential binding of avian virus to neuronal cells of humans and mice.

Mouse-adapted H9N2 influenza virus acquired neurovirulence

To study neuronal adaptation of AIVs, we passaged an H9N2 virus (A/chicken/Shandong/16/05; SD16) in BALB/c mice via the intranasal (i.n.) route, at 10^6 egg infectious dose (EID_{50}) of virus per mouse. By passage 13 (P13), the mouse-adapted (MA)-H9N2 virus infected mice exhibited clear signs of depression and tremor. Histopathology examined showed that SD16 virus-infected brain appeared normal (Fig. 2B), but SD16-MA virus-infected brain showed typical symptoms of encephalitis, characterized by infiltrating inflammatory cell surrounding the blood vessels and neuronophagia (Fig. 2C). By immunohistochemistry (IHC), viral antigens were detected in neurons and glial cells of SD16-MA virus-infected brain (Fig. 2F and 2I), but not with the parental (P0) virus (Fig. 2E and 2H), indicating that the SD16 virus have gained neurotropism. P13 MA virus recovered

from brain of infected mice was plaque purified three times in Madin-Darby canine kidney (MDCK) cells; one clone, SD16-MA, was used for further studies.

Neurotropic virus more pathogenic in mice

Influenza patients with CNS manifestations are more likely to experience severe illness with unfavourable outcome (27). To assess neurotropic pathogenicity of MA-H9N2 virus, each of two groups of eight BALB/c mice was i.n. inoculated with SD16 or SD16-MA virus at the dose of 10^6 EID_{50}/mouse. Clinical signs, mortality and body weight loss were monitored over 14 days. Mice infected with SD16-MA exhibited clear signs of depression (huddling, tremor, decreased activity, wheezing and ruffled fur); by 6 day post-infection (dpi) all mice died. (Fig. 3A and B). By contrast, mice infected with SD16 showed only moderate weight loss at 18.7% and all mice regained weight from 8 dpi (Fig. 3A and B). SD16-MA virus titers in the lungs at 5 dpi were at least 10-fold higher than those derived from parental SD16 virus infection (Fig. 3C). Crucially, SD16-MA virus could be isolated from the brains of infected mice (mean titers of 3.2 $\log_{10}$ EID_{50} /ml at 5 dpi) but no virus was detected from those of SD16 virus-infected mice (Fig. 3C). These results indicate that SD16-MA H9N2 virus produced higher viral titers and become neurotropic in mice.

Neurovirulence of mouse-adapted H9N2 virus associated with mutations located in PB2 and HA genes

To identify adaptive viral gene changes in SD16-MA associated with neurovirulence, 30 plaque clones of SD16-MA, randomly picked, were sequenced and compared with the parental SD16 virus. Eight consensus mutations were identified in five viral proteins: PB2 (M147L, V250G and E627K), PB1 (Y657H), HA (R211K and L226Q, H3 number), M1 (R210K) and NS1 (L214F) (Table 1). To determine the functional

effect of the SD16-MA mutations, five recombinant viruses were constructed, each with a single SD16-MA segment, in the parental SD16 background: rSD16-MA/PB2, rSD16-MA/PB1, rSD16-MA/HA, rSD16-MA/M1 and rSD16-MA/NS1. rSD16 and rSD16-MA were also generated by reverse genetics for inclusion as controls. Groups of eight BALB/c mice were i.n. inoculated with each recombinant virus at the dose of 10^6 EID_{50}. Clinical signs, mortality and body weight loss of five mice were monitored over 14 days. Brains and lungs were collected from 3 BALB/c mice per group at 5 dpi for virus titration. Mice infected with rSD16-MA, rSD16-MA/PB2 and rSD16-MA/HA virus showed 25% to 28 % weight loss and 100% mortality by 8 dpi (Fig. 4A and 4B). On the contrary, similar to rSD16 virus infection, all mice infected with rSD16-MA/PB1, rSD16-MA/M1 and rSD16-MA/NS1 viruses survived with maximum 18% weight loss (Fig. 4A and 4B). Like the P13 SD16-MA virus, rSD16-MA virus was detected in brain in all 3 mice (100% isolation rate) at an average titer of 3.1± 0.3 $\log_{10}$ EID_{50}/ml; rSD16 was not detected in any mice brain (Fig. 4C). Of the 5 recombinants, only rSD16-MA/PB2 and rSD16-MA/HA viruses were detected in 2/3 mice with average virus titers of 2.25-2.75 $\log_{10}$ EID_{50}/ml (Fig. 4C). Virus titer in lungs result showed that rSD16-MA infected group showed highest virus titer with about 6.9 $\log_{10}$ EID_{50}/ml. When infected with rSD16-MA/PB2 and rSD16-MA/HA, the virus titer in lungs is 6.4 and 6.3 $\log_{10}$ EID_{50}/ml respectively. While there's no significant difference of the virus titer of lungs in rSD16-MA/PB1, rSD16-MA/M1 and rSD16-MA/NS1 infected groups compared with in rSD16 infected group (5.1-5.4 $\log_{10}$ EID_{50}/ml, Fig. 4D). Thus, the mutations sited in PB2 and HA are closely involved in neurovirulence and pathogenicity of the MA H9N2 virus (SD16-MA).

Mouse-adapted H9N2 virus reverted back to SA-α2, 3 receptor binding preference

The binding specificity of HA to host receptor is a critical determinant for influenza virus cell attachment and entry (17). AIVs typically show binding affinity for the SA-α2, 3 Gal receptor, however, many naturally occurring avian H9N2 viruses have acquired the ability to preferentially bind to the SA-α2, 6 Gal receptor (13). HA 226L confers SA-α2, 6 Gal receptor binding preference, whereas HA 226Q virus prefers SA-α2, 3 Gal receptor binding (28). The two HA mutations identified in the SD16-MA virus are sited at the receptor-binding pocket: one being the avian-like HA 226Q. Direct binding assays with SA-α2, 3Gal and SA-α2, 6Gal sialylglycopolymers showed that parental rSD16 virus and rSD16-MA/HA virus preferably bound SA-α2, 6 Gal receptor and SA-α2, 3 Gal receptor respectively (Fig. 5A). The reversal adaptation of HA in rSD16-MA virus to facilitate binding to avian-type SA-α2, 3 Gal receptor could make the virus more able to infect avian-like receptor-enriched neuronal cells. Mouse neuroblastoma (N2a) cells infected separately with rSD16 and rSD16-MA/HA viruses (at a multiplicity of infection (MOI) of 0.1) for 16 h showed viral NP protein presence in 34% and over 95% of cells respectively ($P < 0.05$) (Fig. 5B). Thus, rSD16-MA/HA virus appears better adapted than rSD16 to replicate in neuronal cells.

Mouse-adapted PB2 promoted its nuclear import and raised viral RNP polymerase activity.

PB2 protein, synthesized in the cytoplasm, is imported into nucleus to form part of a multiprotein RNP polymerase complex with PB1, PA and NP (29). At 4 hour post-infection (hpi), detection of nuclear import of PB2 protein from SD16-MA/PB2

virus infection of N2a cells was earlier than that of SD16 virus at 6 hpi (Fig. 6A). At 8 and 10 hpi, nuclear detection of PB2 protein in cells infected with rSD16-MA/PB2 virus was at 68% and 87% respectively; corresponding nuclear detection of PB2 from rSD16 virus infection was lower at 26% and 52% respectively ($P < 0.05$) (Fig. 6B). Furthermore, Western blotting of nuclear protein extracts from time-course infection of N2a cells clearly showed earlier and greater PB2 protein accumulation with rSD16-MA/PB2 virus infection than that of parental rSD16 virus (p-value < 0.05) (Fig. 6C). Thus, PB2 gene in rSD16-MA PB2 virus conferred earlier and higher nuclear accumulation of its PB2 protein relative to that of parental PB2 gene from rSD16 virus.

Viral RNP assays (29)were performed in 293T cells to compare PB2-associated polymerase function of rSD16 virus and rSD16-MA/PB2 virus. Polymerase activity derived from rSD16-MA/PB2 virus was 37-fold higher than that from rSD16 virus (Fig. 7A). Western blotting based on corresponding protein lysates did not detect any quantitative difference between the two PB2 proteins (Fig. 7B). Thus, the higher polymerase activity associated with MA PB2 was due to raised enzymatic activity. Taken together, MA PB2 increased its nuclear import (temporal and spatial) efficiency and RNP polymerase activity, which could facilitate infection of neuronal cells.

PB2 and HA from mouse-adapted H9N2 virus individually promoted increase in virus replication and NP protein production in neuronal cells

The replication profiles of three neurovirulent viruses (rSD16-MA, rSD16-MA/PB2 and rSD16-MA/HA) in N2a cells were compared with control rSD16 virus over a time course of 72 h. Throughout the monitoring period at 2, 12, 24, 36, 48, 60 and 72 hpi, all three neurovirulent viruses produced much greater progeny virus (close to

1000-fold greater) ($P < 0.001$) than that of rSD16 virus (Fig. 8A). Expression of NP protein, a major component of the RNP complex (29, 30), of each neurovirulent virus at 24 hpi was also higher than that of corresponding rSD16 control in N2a cells (Fig. 8B). Thus, rSD16-MA/HA and rSD16-MA/PB2 viruses were more replication proficient in N2a cells than parental rSD16 virus.

FMRP is a critical host factor in mouse-adapted H9N2 virus infection of murine brain

FMRP is an RNA-binding protein that interacts with NP protein to promote viral RNP assembly in an RNA-dependent manner (30). FMRP is abundant in "fragile X granules" in neuronal axons and presynaptic terminals where it seems to regulate recurrent neuronal activity (31). To assess the involvement of FMRP in influenza virus replication in neuronal cells, groups of (*FMRP*$^{-/-}$) and wild type (WT) mice (FVB strain background), 11 mice per group, were i.n. infected with rSD16-MA (at 10^6 EID_{50}/mouse). Clinical signs, mortality and body weight loss of 5 mice were monitored over 14 days. Brains and lungs were collected from 3 mice per group at 3 and 5 dpi for virus titration. *FMRP*$^{-/-}$ and WT mice infected with rSD16-MA virus exhibited severe clinical signs, including huddling, decreased activity and wheezing, all the mice showed more than 25% weight loss and 100% mortality by 6 dpi (Fig. 9A). The virus replicated to comparable titers in the lungs of both genotypes (all above 4 $\log_{10}$ EID_{50}/ml). However, in the brains of WT mice, virus titer at 5 dpi (Fig. 9B) was significantly higher (at 3.1±0.3 $\log_{10}$ EID_{50}/ml) than those of *FMRP*$^{-/-}$ murine brains; *FMRP* RNA expression was correspondingly more abundant (19.6 fold higher) in WT murine brain than lung (GAPDH was used to normalize the input samples by the $2^{-\Delta\Delta CT}$ method, Fig. 9C). Thus, FMRP appears to facilitate rSD16-MA virus

replication in the murine brain but not in the lung.

Primary neuronal cortical cells derived from *FMRP*$^{+/+}$ and *FMRP*$^{-/-}$ mice were infected with 0.1 MOI of rSD16-MA for 72 h. Viral titers monitored from 12 to 72 hpi consistently showed *FMRP*$^{+/+}$ cells produced more progeny virus (up to $10^{2.75}$-fold higher) than *FMRP*$^{-/-}$ cells (Fig. 9D). *FMRP*$^{+/+}$ cells infected for 6 h with rSD16-MA (at 1.0 MOI) exhibited more abundant infectious foci at 38.7%, as determined by viral NP immunodetection, than corresponding *FMRP*$^{-/-}$ cells at 3.7% (Fig. 9E). Taken together, FMRP promotes rSD16-MA virus replication in primary murine neurons.

FMRP and NP protein association promotes NP export from the nucleus in rSD16-MA virus infected neuronal cells

As NP protein was more highly expressed with rSD16-MA virus than rSD16 virus infection in N2a cells (Fig. 8B), FMRP-NP interaction was examined by co-immunoprecipitation with anti-NP antibody for each virus infection. Association between NP protein and FMRP was detected with rSD16-MA virus infection but not with rSD16 virus (Fig. 10). The detectable interaction between FMRP and NP from rSD16-MA virus was associated with higher NP protein expression (Fig. 10).

Since the interaction of FMRP and NP facilitates vRNP export from nucleus (30), we assessed this functional association in neuronal cells. FMRP in human neuroblastoma cells (SH-SY5Y) was stably knocked down by shRNAs (Fig. 11A). WT and FMRP knock-down SH-SY5Y cells infected with rSD16-MA (at 2.0 MOI) were examined for nuclear presence of NP over 12 hpi by confocal microscopy. At 12 hpi, significantly more nuclei of FMRP knock-down cells contained NP protein than WT cells (Fig. 11B and 11C). Thus, FMRP and NP association is involved in the nuclear export of NP protein in SH-SY5Y cells. Taken together, the stronger

283 expression of NP protein from rSD16-MA virus infection promotes FMRP-NP
284 interaction which in turn facilitates NP export from the nucleus of infected neuronal
285 cells.

286 **FMRP is required for replication of neurotropic H5N1 and H10N7 viruses in**
287 **murine brain**

288 To determine whether FMRP supports other influenza subtypes in neuronal virus
289 replication, FMRP knockout (*FMRP*$^{-/-}$) and wild type (WT) mice were infected
290 separately with two neurotropic viruses: H5N1 virus (22) and a mouse-adapted
291 H10N7 virus (32) at 10^6EID$_{50}$/mouse. Brains and lungs of 3 mice from each group
292 were collected at 3 and 5 dpi for virus isolation. H5N1 and H10N7-MA viruses
293 replicated efficiently in WT mice brains with the average titer of 3.1 $\log_{10}$ EID$_{50}$/ml
294 and 2.5 $\log_{10}$ EID$_{50}$/ml respectively at 5 dpi. In *FMRP*$^{-/-}$ mice, neither H5N1 virus nor
295 H10N7-MA virus could be detected at 5 dpi (Fig. 12A). However, these viruses could
296 replicate efficiently in mice lungs and no significant difference of virus titers (all
297 above 5 $\log_{10}$ EID$_{50}$/ml) was found between WT and *FMRP*$^{-/-}$ groups ($P > 0.05$),
298 indicated that the FMRP is not indispensable for AIVs replication in mice lungs (Fig.
299 12B). These results demonstrated that the FMRP is a necessary host factor for the
300 replication of neurotropic AIVs in the murine brain but not in lungs.

301 **DISCUSSION**

302 AIVs are zoonotic viruses that exhibit a range infectivity and severity in the human
303 host. Severe human cases of AIV infection are often accompanied by neurological
304 symptoms. In this study, we discovered that avian-like SA-α2, 3 Gal receptor is highly
305 represented in mammalian (human and mouse) brains, and, in the generation of a
306 mouse-adapted neurotropic H9N2 AIVs, identified key adaptive mutations in its HA

and PB2 genes that conferred neurotropism and neurovirulence in mice. We further established that host FMRP protein, highly enriched in the brain, physically associates with viral NP protein in the assembly and export of RNP complex, is a necessary host factor for neurotropic AIVs (H9N2, H5N1 and H10N7 viruses) to undertake neuronal replication.

Influenza virus neurovirulence, characterized by the ability to gain entry and subsequent replication in the CNS, could be found in some influenza virus infected cases with severe illness (33-35). However, little is known about the adaptive strategy of AIVs for neurovirulence. Here, we generated a neurovirulent H9N2 influenza (SD16-MA) virus through repeated passage in mice. SD16-MA virus showed binding affinity for SA-α2, 3 Gal receptor, a reversal from previous SA-α2, 6 Gal receptor binding preference, and was more replicative than parental SD16 virus in neuronal N2a cells. The two HA mutations (R211K and L226Q) of SD16-MA virus are located around the HA receptor-binding pocket; 226Q is a known critical determinant for avian-like SA-α2, 3 Gal receptor binding (26). We also showed that another reassortant rSD16-MA/PB2 virus, without the binding affinity for SA-α2, 3 Gal receptor of SD16-MA virus, replicated effectively in the murine brain. Thus, SA-α2, 3 Gal receptor binding specificity appears to facilitate cell entry but is not indispensable in neurotropic adaptation of SD16-MA virus.

The three mutations (M147L, V250G and E627K) identified in PB2 of SD16-MA virus are associated with increased RNP activity, promotion of PB2 protein production and its nuclear import, and culminating in increased progeny virus production from infected neuronal cells. PB2-E627K is a well characterized PB2 mutation that mediates increased polymerase activity, replication and pathogenicity in

mammals (36-38). E627K is frequently found in avian H5N1 and H7N9 virus strains isolated from humans (36-38) and in H9N2 viruses from infected mice (13). A role of PB2 627K in neurovirulence was also demonstrated in H5N1 influenza virus (24). As residues at 147 and 250 position are in the PB2-NP binding and cap binding domains, they could functionally dictate polymerase function and vRNP assembly. In summary, HA and PB2 genes from mouse-adapted H9N2 (SD16-MA) virus, separately introduced into a parental SD16 virus backbone, can result in neurovirulent infection in mice.

In addition to the identification of HA and PB2 mutations that are responsible for neurovirulence in a mouse-adapted avian H9N2 (SD16-MA) virus, we identified FMRP as an essential host factor that mediates neurovirulence, without which neurotropic H9N2, H5N1 and H10N7 influenza viruses are unable to replicate in the brain. FMRP forms part of a large RNP complex that is involved in the transport and translation of mRNA in neurons (39); it was previously shown that FMRP stimulated replication of human influenza A/PR/8/34 (PR8) virus in the upper respiratory tract of mice through RNA-mediated interaction with NP protein (30). However, FMRP is not required to support SD16-MA virus replication in the murine lung. The absence or specific mutation(s) of FMRP leads to Fragile X syndrome and causes inherited mental retardation and autism (40). Clinically, the frequency and severity of influenza virus infection in individuals with FMR1 mutations need to be paid more attention.

In summary, the adaptive mutations of HA and PB2 that improve host receptor affinity, enhance viral polymerase activity and facilitate nucleocytoplasmic shuttling of viral proteins are the key changes needed by AIVs to achieve neurovirulence in mice, which, in turn, is contingent on the interaction between host FMRP and viral NP

protein to effect neuronal virus replication.

MATERIALS AND METHODS

Ethics Statement

All animal work was approved by the Beijing Association for Science and Technology (approval ID SYXK [Beijing] 2007-0023) and conducted in accordance with the Beijing Laboratory Animal Welfare and Ethics guidelines, as issued by the Beijing Administration Committee of Laboratory Animals, and in accordance with the China Agricultural University (CAU) Institutional Animal Care and Use Committee guidelines (ID: SKLAB-B-2010-003).

Cells and viruses

Human embryonic kidney (293T) cells, mouse N2a cells and human neuroblastoma (SH-SY5Y) cells were maintained in Dulbecco's modified Eagle's medium (DMEM; Life Technologies) supplemented with 10% fetal bovine serum (FBS; Life Technologies), 100 units/ml of penicillin and 100 μg/ml of streptomycin.

The influenza viruses of WT (parental) H9N2 (A/chicken/Shandong/16/05 (SD16)), H5N1 (A/chicken/Sheny/0606/2008) and H10N7-MA (mouse adapted A/mallard/Beijing/27 /2011) was previously described (22, 32, 41). Virus titers were measured by 50% tissue culture infectious dose ($TCID_{50}$) assay in MDCK cells or EID_{50} assay in eggs (42). All experiments with H5 subtype viruses were performed in biosafety level 3 containment.

Isolation and cultural of Murine primary neuron cortical cells

Whole cerebral cortices were removed from FVB neonatal mice (1-2 days), taking

care to discard the hippocampal formation, basal ganglia, most of meninges and vessels. The tissue was minced, incubated in 2mg/ml papain supplement (Sigma) with 0.05mg/mL DNase (Sigma) for 45-60 min at 37°C, dissociated by trituration, and plated as a single-cell suspension on lysine (Sigma) treated 6-well plate (3×10^6 cells/well) in a plating medium of DMEM: Nutrient Mixture F-12 (DMEM/F12, Gibco) supplemented with 10% FBS, 0.5% penicillin-streptomycin solution (Thermo Fisher Scientific) and 1% B27 supplement (Gibco). The plates were maintained at 37°C in a humidified 5% CO_2 atmosphere. After 24h in vitro, replace the plating medium with cell culture medium neurobasal-A supplemented (Thermo Fisher Scientific) with 0.5mmol/L L-glutamine (Thermo Fisher Scientific), 0.5% penicillin-streptomycin Solution and 1% B27 supplement). After 48h, replace the old cell culture medium with cell culture medium containing 10μmol/L cytosine arabinoside (MedChem express). Subsequent media replacement was carried out every 48h. 6-7 days after isolation, cells could be used for infection assays.

Adaptation of H9N2 virus in mice

Groups of three BALB/c mice (6-week-old female BALB/c; Vital River Laboratory) were lightly anesthetized with Zoletil 50 (Tiletamine-zolazepam; Virbac S.A. 20 mg/g) and inoculated i.n. with 10^6 EID_{50} of viruses in 50 μl phosphate buffered saline (PBS, Gibco). At 3 dpi, three inoculated mice were euthanized, and the lungs were harvested and homogenized in 2ml of sterile cold PBS, 50 μl of supernatant from the centrifuged homogenate was used as inoculum for the next passage. After 13 passages, the virus could be isolated in brain from infected mice. The virus isolated from brain was cloned three times by plaque purification in MDCK cells, and the cloned virus was passaged once in the allantoic cavities of 10-day-old embryonated chicken eggs

401 at 37^{o}C for 72 h to generate virus stock.

402 **Sequence analysis**

403 The virus present in the brain from the 13 passage virus infected mice was plaque
404 purified three times in MDCK cells. Thirty clones were chosen randomly for
405 sequencing. Viral RNAs were extracted from the allantoic fluid of the 30 clones
406 infected eggs and the eight viral genes of each strain were amplified by reverse
407 transcription-PCR (RT-PCR). The segments were sequenced and adaptive mutations
408 were identified by comparing the consensus sequences of the 30 clones to the
409 sequences of WT SD16 virus.

410 **Plasmid construction and virus rescue**

411 All eight gene segments were amplified by reverse transcription-PCR (RT-PCR) from
412 SD16 and SD16-MA viruses and cloned into the dual-promoter plasmid, pHW2000.
413 All of the constructs were sequenced to confirm the mutations. rSD16,
414 rSD16-MA/PB2, rSD16-MA/HA, rSD16-MA/PB2-HA, rSD16-MA/M1,
415 rSD16/MA-NS1 and rSD16-MA were generated by reverse genetics. Briefly, 0.5 μg
416 of plasmid for each gene segment was mixed and incubated with 8 μl of TransIT-LT1
417 reagent (Mirusbio, USA) at 25°C for 30 min. The TransIT-LT1-DNA mixture was
418 transferred to 70% confluent 293T cultured monolayers and incubated at 37°C with 5%
419 CO_2. 6 hpi, the supernatants were replaced with 2 ml of OPTI-MEM containing 2
420 μg/ml tosylsulfonyl phenylalanyl chloromethyl ketone (TPCK) treated trypsin
421 (Sigma-Aldrich). 48 hpi, the cell suspension were harvested and inoculated into
422 10-day-old SPF eggs and held for 72 h at 37°C to prepare a virus stock. Viral RNA
423 was extracted and analyzed by RT-PCR, and each viral segment was sequenced to
424 confirm the sequence identity.

Virus titration and replication kinetics

$TCID_{50}$ was determined in MDCK cells with 10-fold serially diluted viruses inoculated at 37°C for 72 h. The $TCID_{50}$ value was calculated by the Reed-Muench method. Multistep replication kinetics was determined by inoculating N2a and Murine primary neuron cortical cells viruses at an MOI of 0.1. After 1 h of incubation at 37°C, the cells were washed twice and further incubated in serum-free DMEM containing 1 μg/ml tTPCK trypsin (Sigma). Supernatants were sampled at 2, 12, 24, 36, 48, 60, and 72 hpi. All collected supernatants were titrated on MDCK cells; three independent experiments were performed.

Mouse experiments

6-week-old male WT and *FMR1*-gene knockout ($FMRP^{-/-}$) mice in the FVB.129P2 (B6)-Fmr1tm1Cgr/J strain background were bought from Chinese Academy of Medical Sciences. Mice were genotyped and the lack or presence of the Fmr1 gene was confirmed by PCR by Chinese Academy of Medical Sciences.

Groups of 6-week-old female BALB/c mice were anesthetized with Zoletil 50 (Virbac S.A) and inoculated i.n. with 10^6 EID_{50} of viruses in 50 μl PBS. Three mice in each group were euthanized at 3 and 5 dpi. Lungs and brains were collected for virus titration in SPF eggs. The remaining five mice in each group were monitored for weight loss and mortality for 14 days. Mice that lost more than 25% of their body weight were humanely euthanized.

Western blotting

Total cell protein were extracted from transfected 293T cells or infected N2a cells with RIPA lysis buffer and total protein concentration was determined by a BCA

protein assay kit (Beyotime). Cellular proteins were separated by 12% sodium dodecyl sulfate-polyacrylamide gel electrophoresis (SDS-PAGE) and transferred to a polyvinylidene difluoride (PVDF) membrane (Bio-Rad). Each PVDF membrane was blocked with 0.1% Tween 20 and 5% non-fat dry milk in PBS and subsequently incubated with a primary antibody. Primary antibodies were specific for influenza A virus PB2 (diluted 1:1000, GenScript, China), NP (diluted 1:1000, Abcam), and host protein FMRP (diluted 1:1000, Abcam). Secondary antibody used was horseradish peroxidase (HRP)-conjugated anti-rabbit or anti–mouse antibody (diluted 1:10,000, Beyotime). HRP presence was detected using a Western Lightning chemiluminescence kit (Amersham Pharmacia), following the manufacturer's protocols.

Viral ribonucleoprotein polymerase assay

RNP polymerase (mini genome luciferase) assays were based on the co-transfection of four pcDNA3.1 expression plasmids housing PB1, PA, NP with PB2 or PB2-MA into human 293T cells (125ng of each plasmid), together with a pYH-NS1-Luci plasmid expressing a reporter firefly luciferase gene under the control of the human RNA polymerase I promoter (10 ng), and an internal control plasmid expressing renilla (2.5 ng). Cultures were incubated at 37 °C. After 24 h of transfection, cell lysates were prepared with Dual Luciferase Reporter Assay System (Promega), and luciferase activity was determined in a GloMax 96 microplate luminometer (Promega).

RNA isolation and quantitative RT-PCR

Groups of 6-week-old female BALB/c mice were anesthetized with Zoletil 50 (Virbac S.A), brains and lungs from 3 mice were collected. Total RNA was isolated from each

collected tissue with RNA isolation reagent (Thermo Fisher) in accordance with the instruction of the manufacturer. The RNAs were reverse transcribed into cDNA by TransScript RT reagent Kit (TransGen). Oligo dT primers were used for detecting the FMRP gene. The obtained cDNA was amplified by a fast two-step amplification using FastStart Universal SYBR Green Master mix (Roche, China). GAPDH was used to normalize the input samples by the $2^{-\Delta\Delta CT}$ method. For detection of FMRP and GAPDH, primers of 5'- GAGATCGTGGACAAGTCAGGAG-3' (FMRP forward), 5'- CTTCAGAGGAGTTAGGTCCAACC-3' (FMRP reverse), 5'- ACAACTTTGGCAT TGTGGAA-3' (GAPDH forward) and 5'- GATGCAGGGATGATGTTCTG -3' (GAPDH reverse) were used in this study.

Co-immunoprecipitation assay

N2a cells were infected separately with 0.1 MOI of rSD16 virus and rSD16-MA virus. 24 h later, cells were washed with cold PBS and lysed in RIPA buffer (Beyotime). The lysates were incubated with anti-NP (diluted 1:250, Abcam) antibody at 4°C for 16 h, and the protein G PLUS-Agarose (Santa Cruz) were then added and rotated at 4°C for 6h. The beads were washed 6-7 times with lysis buffer, and the bound proteins were separated by SDS-PAGE followed by Western blotting with the indicated antibody.

Lectin histochemistry

Each mouse was perfused transcardially with 10-20 ml of PBS followed by 20 ml of freshly prepared 4% paraformaldehyde. The brains were removed and post-fixed in 4% paraformaldehyde at room temperature for more than 24 hours and less than 48 hours. Both sagittal and transverse sections of the brains were prepared. For detection of host influenza receptors in the tissues, the organs were sectioned at 4-μm thickness. The human brain tissue sections are provided by Beijing Longmaidasi technology

development. Detection details of host influenza receptors are found in Kuchipudi et al (43). Briefly, sections were pre-soaked in Tris-buffered saline (TBS) and blocked using a biotin-streptavidin blocking kit (Vector Laboratories) according to manufacturer's instructions, followed by overnight incubation at 4°C with biotinylated SNA (Vectorlabs) or FITC labelled MAL I (Vectorlabs), each at a concentration of 10μg /ml. After three washes with TBS, the sections were incubated with streptavidin-Alexa-Fluor594 conjugate (Invitrogen) for 2 h at room temperature. The sections were washed and mounted with ProLong Gold anti-fade reagent with 4', 6-diamino-2-phenylindole, dihydrochloride (DAPI; Invitrogen).

Virus detection by immunofluorescence

N2a cells were grown on the carry sheet glass in 24 well plate and infected with the indicated viruses. At the specified time points post infection, the cells were fixed with 4% paraformaldehyde in PBS for 30 min and permeabilized with 0.5% Triton X-100 in PBS for 30 min. After blocking with 5% bovine serum albumin (BSA) in PBS, the cells were incubated with antisera against PB2 (diluted 1:500, GeneTex) or NP (diluted 1:500, Abcam) at 4°C for 12 h. The cells were then washed three times with PBS and incubated with goat anti-rabbit (FITC) (diluted 1:500, Abcam) or goat anti-rabbit IgG (Alexa Fluor 594) (diluted 1:500, Abcam) secondary antibodies for 1 h at 37°C. The cells were subsequently washed three times with PBS and incubated with DAPI for 10 min. Cells were imaged with a laser scanning confocal microscope (Leica). The frequency of nuclear localization of the PB2 protein was determined by cell counting (n=100).

RNA interference

Cells were transfected with siRNAs at 50nM for indicated times. The following

sequences were targeted for FMR1 (5'-3'): #1: 5'-CCAAAGAGGCGGCACAUA A-3'; #2: 5'-AAAGCUAUGUGACUGAUGA-3'; #3: 5'-CAGCUUGCCUCGA GAUUUC-3'. Lentivirus expressing FMRP-specific short-hairpin RNA was generated by the GenePharma Company (Shanghai). Briefly, two complementary oligonucleotides with *BamH*I and *EcoR*I endonuclease sites at each end were synthesized, annealed and cloned into a HIV-based lentiviral expression vector (LV3-pGLV-H1-GFP/ PURO, GenePharma, Shanghai) to express a hairpin transcript (5'-GCAGCTTGCCTCGAGATATCTCAAGAGGATATCTCGAGGCAAGCTGC TT-3'). The lentiviral particles were then produced by co-transfecting the short-hairpin RNA expression plasmids with packaging plasmids into 293 packaging cells. After 72 h, viruses were collected and titered. To generate FMRP-stable knockdown or control cell lines, SH-SY5Ycells were infected with the lentiviral particles and selected with puromycin (1 mg/ml) for 3 weeks.

Statistical analyses

All statistical analyses were performed using GraphPad Prism software version 5.00 (GraphPad Software Inc.). Statistically significant differences between experimental groups were determined using the Dunnett's test following one-way ANOVA. Differences were considered statistically significant at $P < 0.05$.

ACKNOWLEDGMENTS

This work was supported by the National Key Research and Development Program (2016YFD0500204) and National Natural Science Foundation of China (Program 31873022).

REFERENCES

1. Chen H, Yuan H, Gao R, Zhang J, Wang D, Xiong Y, Fan G, Yang F, Li X, Zhou J, Zou S, Yang L, Chen T, Dong L, Bo H, Zhao X, Zhang Y, Lan Y, Bai T, Dong J, Li Q, Wang S, Zhang Y, Li H, Gong T, Shi Y, Ni X, Li J, Zhou J, Fan J, Wu J, Zhou X, Hu M, Wan J, Yang W, Li D, Wu G, Feng Z, Gao GF, Wang Y, Jin Q, Liu M, Shu Y. 2014. Clinical and epidemiological characteristics of a fatal case of avian influenza A H10N8 virus infection: a descriptive study. Lancet 383:714-21.
2. Pan M, Gao R, Lv Q, Huang S, Zhou Z, Yang L, Li X, Zhao X, Zou X, Tong W, Mao S, Zou S, Bo H, Zhu X, Liu L, Yuan H, Zhang M, Wang D, Li Z, Zhao W, Ma M, Li Y, Li T, Yang H, Xu J, Zhou L, Zhou X, Tang W, Song Y, Chen T, Bai T, Zhou J, Wang D, Wu G, Li D, Feng Z, Gao GF, Wang Y, He S, Shu Y. 2016. Human infection with a novel, highly pathogenic avian influenza A (H5N6) virus: Virological and clinical findings. J Infect 72:52-9.
3. Gao R, Cao B, Hu Y, Feng Z, Wang D, Hu W, Chen J, Jie Z, Qiu H, Xu K, Xu X, Lu H, Zhu W, Gao Z, Xiang N, Shen Y, He Z, Gu Y, Zhang Z, Yang Y, Zhao X, Zhou L, Li X, Zou S, Zhang Y, Li X, Yang L, Guo J, Dong J, Li Q, Dong L, Zhu Y, Bai T, Wang S, Hao P, Yang W, Zhang Y, Han J, Yu H, Li D, Gao GF, Wu G, Wang Y, Yuan Z, Shu Y. 2013. Human infection with a novel avian-origin influenza A (H7N9) virus. N Engl J Med 368:1888-97.
4. Claas EC, Osterhaus AD, van Beek R, De Jong JC, Rimmelzwaan GF, Senne DA, Krauss S, Shortridge KF, Webster RG. 1998. Human influenza A H5N1 virus related to a highly pathogenic avian influenza virus. Lancet 351:472-7.
5. Zhao G, Gu X, Lu X, Pan J, Duan Z, Zhao K, Gu M, Liu Q, He L, Chen J, Ge S, Wang Y, Chen S, Wang X, Peng D, Wan H, Liu X. 2012. Novel reassortant highly pathogenic H5N2 avian influenza viruses in poultry in China. PLoS One 7:e46183.
6. Wu H, Lu R, Peng X, Xu L, Cheng L, Lu X, Jin C, Xie T, Yao H, Wu N. 2015. Novel reassortant highly pathogenic H5N6 avian influenza viruses in poultry in China. Infect Genet Evol 31:64-7.
7. Fan S, Zhou L, Wu D, Gao X, Pei E, Wang T, Gao Y, Xia X. 2014. A novel highly pathogenic H5N8 avian influenza virus isolated from a wild duck in China. Influenza Other Respir Viruses 8:646-53.
8. Lam TT, Wang J, Shen Y, Zhou B, Duan L, Cheung CL, Ma C, Lycett SJ, Leung CY, Chen X, Li L, Hong W, Chai Y, Zhou L, Liang H, Ou Z, Liu Y, Farooqui A, Kelvin DJ, Poon LL, Smith DK, Pybus OG, Leung GM, Shu Y, Webster RG, Webby RJ, Peiris JS, Rambaut A, Zhu H, Guan Y. 2013. The genesis and source of the H7N9 influenza viruses causing human infections in China. Nature 502:241-4.
9. Su S, Gu M, Liu D, Cui J, Gao GF, Zhou J, Liu X. 2017. Epidemiology, Evolution, and Pathogenesis of H7N9 Influenza Viruses in Five Epidemic Waves since 2013 in China. Trends Microbiol 25:713-728.
10. FAO. http://www.fao.org/ag/againfo/programmes/en/empres/h7n9/situation_update.html.
11. Wang B, Chen Q, Chen Z. 2012. Complete genome sequence of an H9N2 avian influenza virus isolated from egret in Lake Dongting wetland. J Virol 86:11939.
12. Xu KM, Smith GJ, Bahl J, Duan L, Tai H, Vijaykrishna D, Wang J, Zhang JX, Li KS, Fan XH, Webster RG, Chen H, Peiris JS, Guan Y. 2007. The genesis and evolution of H9N2 influenza viruses in poultry from southern China, 2000 to 2005. J Virol 81:10389-401.
13. Li X, Shi J, Guo J, Deng G, Zhang Q, Wang J, He X, Wang K, Chen J, Li Y, Fan J, Kong H, Gu C, Guan Y, Suzuki Y, Kawaoka Y, Liu L, Jiang Y, Tian G, Li Y, Bu Z, Chen H. 2014. Genetics, receptor binding property, and transmissibility in mammals of naturally isolated H9N2 Avian Influenza

viruses. PLoS Pathog 10:e1004508.
14. Yang Y, Liu M. 2011. Analysis of clinical characteristics of human infected with H5N1 highly pathogenic avian influenza. Disease Surveillance 26:328-333.
15. Gu J, Xie Z, Gao Z, Liu J, Korteweg C, Ye J, Lau LT, Lu J, Gao Z, Zhang B. 2007. H5N1 infection of the respiratory tract and beyond: a molecular pathology study. The Lancet 370:1137-1145.
16. Ke C, Mok CKP, Zhu W, Zhou H, He J, Guan W, Wu J, Song W, Wang D, Liu J, Lin Q, Chu DKW, Yang L, Zhong N, Yang Z, Shu Y, Peiris JSM. 2017. Human Infection with Highly Pathogenic Avian Influenza A(H7N9) Virus, China. Emerg Infect Dis 23:1332-1340.
17. Matrosovich M, Tuzikov A, Bovin N, Gambaryan A, Klimov A, Castrucci MR, Donatelli I, Kawaoka Y. 2000. Early alterations of the receptor-binding properties of H1, H2, and H3 avian influenza virus hemagglutinins after their introduction into mammals. Journal of virology 74:8502-8512.
18. Yen HL, Aldridge JR, Boon AC, Ilyushina NA, Salomon R, Hulse-Post DJ, Marjuki H, Franks J, Boltz DA, Bush D, Lipatov AS, Webby RJ, Rehg JE, Webster RG. 2009. Changes in H5N1 influenza virus hemagglutinin receptor binding domain affect systemic spread. Proc Natl Acad Sci U S A 106:286-91.
19. Schrauwen EJ, Herfst S, Leijten LM, van Run P, Bestebroer TM, Linster M, Bodewes R, Kreijtz JH, Rimmelzwaan GF, Osterhaus AD, Fouchier RA, Kuiken T, van Riel D. 2012. The multibasic cleavage site in H5N1 virus is critical for systemic spread along the olfactory and hematogenous routes in ferrets. J Virol 86:3975-84.
20. Suguitan AL, Jr., Matsuoka Y, Lau YF, Santos CP, Vogel L, Cheng LI, Orandle M, Subbarao K. 2012. The multibasic cleavage site of the hemagglutinin of highly pathogenic A/Vietnam/1203/2004 (H5N1) avian influenza virus acts as a virulence factor in a host-specific manner in mammals. J Virol 86:2706-14.
21. Sun X, Tse LV, Ferguson AD, Whittaker GR. 2010. Modifications to the hemagglutinin cleavage site control the virulence of a neurotropic H1N1 influenza virus. J Virol 84:8683-90.
22. Zhang Y, Sun Y, Sun H, Pu J, Bi Y, Shi Y, Lu X, Li J, Zhu Q, Gao GF, Yang H, Liu J. 2012. A single amino acid at the hemagglutinin cleavage site contributes to the pathogenicity and neurovirulence of H5N1 influenza virus in mice. J Virol 86:6924-31.
23. Goto H, Wells K, Takada A, Kawaoka Y. 2001. Plasminogen-binding activity of neuraminidase determines the pathogenicity of influenza A virus. J Virol 75:9297-301.
24. Shinya K, Hamm S, Hatta M, Ito H, Ito T, Kawaoka Y. 2004. PB2 amino acid at position 627 affects replicative efficiency, but not cell tropism, of Hong Kong H5N1 influenza A viruses in mice. Virology 320:258-266.
25. Shinya K, Kawaoka Y. 2006. Influenza virus receptors in the human airway. Uirusu 56:85-9.
26. de Graaf M, Fouchier RA. 2014. Role of receptor binding specificity in influenza A virus transmission and pathogenesis. Embo j 33:823-41.
27. Khandaker G, Zurynski Y, Buttery J, Marshall H, Richmond PC, Dale RC, Royle J, Gold M, Snelling T, Whitehead B, Jones C, Heron L, McCaskill M, Macartney K, Elliott EJ, Booy R. 2012. Neurologic complications of influenza A(H1N1)pdm09: surveillance in 6 pediatric hospitals. Neurology 79:1474-81.
28. Wan H, Perez DR. 2007. Amino acid 226 in the hemagglutinin of H9N2 influenza viruses determines cell tropism and replication in human airway epithelial cells. J Virol 81:5181-91.

29. Eisfeld AJ, Neumann G, Kawaoka Y. 2015. At the centre: influenza A virus ribonucleoproteins. Nat Rev Microbiol 13:28-41.
30. Zhou Z, Cao M, Guo Y, Zhao L, Wang J, Jia X, Li J, Wang C, Gabriel G, Xue Q. 2014. Fragile X mental retardation protein stimulates ribonucleoprotein assembly of influenza A virus. Nature communications 5.
31. Akins MR, LeBlanc HF, Stackpole EE, Chyung E, Fallon JR. 2012. Systematic mapping of fragile X granules in the mouse brain reveals a potential role for presynaptic FMRP in sensorimotor functions. Journal of Comparative Neurology 520:3687-3706.
32. Zhang X, Xu G, Wang C, Jiang M, Gao W, Wang M, Sun H, Sun Y, Chang KC, Liu J, Pu J. 2017. Enhanced pathogenicity and neurotropism of mouse-adapted H10N7 influenza virus are mediated by novel PB2 and NA mutations. J Gen Virol 98:1185-1195.
33. Sun G, Ota C, Kitaoka S, Chiba Y, Takayanagi M, Kitamura T, Yamamoto K, Fujie H, Mikami H, Uematsu M. 2015. Elevated serum levels of neutrophil elastase in patients with influenza virus-associated encephalopathy. Journal of the neurological sciences 349:190-195.
34. Surtees R, DeSousa C. 2006. Influenza virus associated encephalopathy. Archives of disease in childhood 91:455-456.
35. Yoganathan S, Sudhakar SV, James EJ, Thomas MM. 2016. Acute necrotising encephalopathy in a child with H1N1 influenza infection: a clinicoradiological diagnosis and follow-up. BMJ case reports 2016:bcr2015213429.
36. Maines TR, Lu XH, Erb SM, Edwards L, Guarner J, Greer PW, Nguyen DC, Szretter KJ, Chen LM, Thawatsupha P, Chittaganpitch M, Waicharoen S, Nguyen DT, Nguyen T, Nguyen HH, Kim JH, Hoang LT, Kang C, Phuong LS, Lim W, Zaki S, Donis RO, Cox NJ, Katz JM, Tumpey TM. 2005. Avian influenza (H5N1) viruses isolated from humans in Asia in 2004 exhibit increased virulence in mammals. J Virol 79:11788-800.
37. Hatta M, Gao P, Halfmann P, Kawaoka Y. 2001. Molecular basis for high virulence of Hong Kong H5N1 influenza A viruses. Science 293:1840-2.
38. Zhang Q, Shi J, Deng G, Guo J, Zeng X, He X, Kong H, Gu C, Li X, Liu J, Wang G, Chen Y, Liu L, Liang L, Li Y, Fan J, Wang J, Li W, Guan L, Li Q, Yang H, Chen P, Jiang L, Guan Y, Xin X, Jiang Y, Tian G, Wang X, Qiao C, Li C, Bu Z, Chen H. 2013. H7N9 influenza viruses are transmissible in ferrets by respiratory droplet. Science 341:410-4.
39. Bagni C, Greenough WT. 2005. From mRNP trafficking to spine dysmorphogenesis: the roots of fragile X syndrome. Nature Reviews Neuroscience 6:376-387.
40. Santoro MR, Bray SM, Warren ST. 2012. Molecular mechanisms of fragile X syndrome: a twenty-year perspective. Annual Review of Pathology: Mechanisms of Disease 7:219-245.
41. Wang J, Sun Y, Xu Q, Tan Y, Pu J, Yang H, Brown EG, Liu J. 2012. Mouse-adapted H9N2 influenza A virus PB2 protein M147L and E627K mutations are critical for high virulence. PLoS One 7:e40752.
42. REED LJ, MUENCH H. 1938. A SIMPLE METHOD OF ESTIMATING FIFTY PER CENT ENDPOINTS12. American Journal of Epidemiology 27:493-497.
43. Kuchipudi SV, Nelli R, White GA, Bain M, Chang KC, Dunham S. 2009. Differences in influenza virus receptors in chickens and ducks: Implications for interspecies transmission. J Mol Genet Med 3:143-51.

672

673

674 **FIGURE LEGEND**

675 **FIG 1** Avian-like SA-α2, 3 Gal receptor appears dominant over human-like SA-α2, 6
676 Gal receptor in murine and human brain. The mouse and human brain tissues were
677 stained with FITC labelled MAL I (SA-α2, 3 Gal receptor, green) or biotinylated SNA
678 (SA-α2, 6 Gal receptor, red); nuclei were stained with DAPI (blue).

679

680 **FIG 2** Mouse-adapted avian H9N2 influenza virus gained neurovirulence in mice.
681 Representative Histological (H.E. stining; left column; A to C) and IHC (right column,
682 D to I) brain sections at day 5dpi are shown. Mouse-adapted H9N2 virus (P13)
683 infected brain showed typical encephalitis, white arrow indicate infiltrating
684 inflammatory cell surrounding the blood vessels. Viral NP protein (brown) were
685 detected in the cerebral tissues of mice infected with mouse-adapted H9N2 virus
686 (P13). Open arrows indicate virus presence in infected brain tissue. Scale bar =
687 200μm.

688

689 **FIG 3** Mouse-adapted avian H9N2 influenza virus gained enhanced pathogenicity in
690 mice. (A) Body weight change (percentage) and (B) survival (percentage) of mice (n
691 = 5 per group) infected separately with SD16 virus and SD16-MA virus, at 10^6
692 EID_{50}/mouse. Body weight change presented as means ± SD of five mice. Mice that
693 lost > 25% of their baseline body weight were euthanized. (C) SD16 virus and
694 SD16-MA virus titers were determined in lungs and brains of infected mice (n = 3 per

group) at 5 dpi. Dashed black line indicates the lower limit of detection ($10^{0.75}$ EID_{50}/ml). Data presented as means ± SD of three mice. (**P < 0.01, ***P < 0.001 as determined by ANOVA).

FIG 4 Mutations in PB2 and HA of mouse-adapted H9N2 virus (rSD16-MA virus) contributed to neurovirulence and enhanced pathogenicity in mice. Mice were infected separately with 10^6 EID_{50} of rSD16, rSD16-MA, rSD16-MA/PB2, rSD16-MA/PB1, rSD16-MA/HA, rSD16-MA/M1 and rSD16-MA/NS1 viruses. (A) Body weight change (percentage) presented as means ± SD of 5 mice and (B) survival (percentage) of mice (n = 5 per group) were monitored in 14 days. Mice that lost > 25% of their baseline body weight were euthanized. Virus titers in the brain (C) and lung (D) were determined at 5 dpi. Each color bar represents virus titer from an individual animal. Dashed black line indicates the lower limit of detection ($10^{0.75}$ EID_{50}/ml).

FIG 5 HA in mouse-adapted H9N2 virus reverted back to avian-like SA-α2, 3 receptor binding preference. (A) Binding affinity of inactivated viruses to SA-α2, 3-linked and α2, 6-linked polymers. Mouse-adapted HA from rSD16-MA virus in parental SD16 virus backbone (rSD16-MA/HA virus) displayed binding affinity for avian-like SA-α2, 3-linked polymers. Control A/Beijing/7/2009 (H1N1) and A/Anhui/1/2005 (H5N1) viruses selectively bound SA-α2, 6- and SA-α2, 3-polymers respectively. Each data point is the mean ±SD of three independent experiments. (B) N2a cells were infected with rSD16 and rSD16-MA/HA viruses at 0.1 MOI. NP protein (red) was detected by immunofluorescence at 16 hpi. Nuclei were stained with DAPI (blue). Scale bar = 50μm.

719

720 **FIG 6** PB2 from mouse-adapted H9N2 virus in rSD16 backbone (rSD16-MA/PB2
721 virus) conferred increased PB2 protein production and its nuclear import. (A)
722 Ten-hour infection time course nuclear localization of PB2 protein (red) in N2a cells
723 infected separately with parental rSD16 virus and rSD16-MA/PB2 virus, each at 2.0
724 MOI. Nuclei were stained with DAPI (blue). Scale bar = 20μm. (B) Relative
725 quantification of PB2 protein nuclear localization. A hundred cells (blue nuclei) were
726 randomly selected from multiple microscopic fields for the presence of intranuclear
727 PB2 (red) was determined. Data are presented as means ± SD of three independent
728 experiments (*$P < 0.05$ as determined by ANOVA). (C) Western blotting of nuclear
729 extracts from correspondingly infected N2a cells to detect nuclear PB2 protein. PCNA
730 immunodetection demonstrated normalized protein loading of each sample.

731

732 **FIG 7** PB2 from SD16-MA (rSD16-MA/PB2 virus) increased viral polymerase
733 activity of parental SD16 virus in 293T cells. (A) Polymerase activity of rSD16 and
734 rSD16-MA/PB2 was determined by minigenome assays. Four protein expression
735 plasmids (PB2, PB1, PA and NP) for RNP constitution of the respective virus were
736 transfected into 293T cells along with luciferase reporter plasmid pYH-Luci and
737 internal control Renilla plasmid. Results presented are means ± SD of three
738 independent experiments and referenced to rSD16 activity set at 100%. (B) Western
739 blotting of cell protein lysates from corresponding transfections harvested at 24 hpi
740 showed no quantitative difference in PB2 protein detection between PB2 genes of
741 sSD16 and rSD16-MA/PB2 viruses (*** $P < 0.001$ as determined by ANOVA).

742

743 **FIG 8** PB2 and HA from SD16-MA virus individually increased expression of NP
744 protein in N2a cells. (A) Cells were infected rSD16, rSD16-MA, rSD16-MA/PB2 and
745 rSD16-MA/HA viruses, each at 0.1 MOI. Supernatants of the infected cells were
746 collected at the indicated time points for virus titration on MDCK cells; virus titers are
747 means ± SD of three independent experiments. Indicated significance relative to
748 corresponding rSD16 virus infection. (B) Infected N2a cells were harvested at 24 hpi
749 for Western blotting detection of NP. Loading normalization evidenced by β-actin
750 detection.

751

752 **FIG 9** FMRP promoted rSD16-MA virus replication in murine brain and primary
753 neuronal cells. *FMRP*$^{-/-}$ and WT mice (FVB strain background) were intranasally
754 infected with 10^6 EID_{50} of rSD16-MA. (A) Body weight change (percentage)
755 presented as means ± SD of 5 mice. Mice that lost > 25% of their baseline body
756 weight were euthanized. (B) Virus titers from brains and lungs of WT and *FMRP*$^{-/-}$
757 mice were determined at 3 and 5 dpi. Dashed black line indicates lower limit of
758 detection ($10^{0.75}$ TID_{50}/ml). (C) Relative expression of *FMRP* mRNA in WT murine
759 brain and lung. Total RNA was extracted from brain and lung tissues of a group of 3
760 BALB/c mice and FMRP mRNA was quantitated by qRT-PCR. GAPDH was used to
761 normalize the input samples by the $2^{-\Delta\Delta CT}$ method. Data presented as the mean ±
762 standard deviation of three independent experiments. (D) *FMRP*$^{+/+}$ and *FMRP*$^{-/-}$
763 primary murine neuron cortical cells were infected with 0.1 MOI of rSD16-MA virus.
764 Virus titers of supernatants, collected at indicated time points, were determined and
765 presented as means ± SD of three independent experiments. (E) *FMRP*$^{+/+}$ and
766 *FMRP*$^{-/-}$ primary cells were infected with rSD16-MA for 6 h for fluorescence

767 immunodetection of NP (green) (DAPI nuclear staining blue). Graph shows detection
768 rate NP positive cells of the two gentoypes. (***$P < 0.001$ as determined by ANOVA).
769 Scale bar = 100μm.

770

771 **FIG 10** Physical interaction of viral NP and host FMRP in N2a cells. Cells were
772 infected separately with rSD16 and rSD16-MA virus, each at 0.1 MOI. At 24 hpi, cell
773 protein lysates were harvested for co-immunoprecipitation and Western blotting as
774 indicated. rSD16-MA virus conferred stronger expression of NP protein than SD16
775 virus, and its NP co-immunoprecipitated with FMRP.

776

777 **FIG 11** FMRP knockdown increased viral NP retention in the nuclei of SH-SY5Y
778 cells infected with rSD16-MA virus. (A) Protein levels of FMRP in wild type
779 SH-SY5Y cells (WT), negative control SH-SY5Y cells (NC) and FMRP-stable
780 knockdown SH-SY5Y cells (shRNA). (B) Relative nuclear localization of NP protein.
781 At least a hundred cells (blue nuclear) from randomly selected microscopic fields of
782 infected SH-SY5Y cells (shRNA and WT) were scored for the presence of
783 intranuclear NP (red) at 8, 10 and 12 hpi. Data are presented as means ± SD
784 deviations of three independent experiments. (* $P < 0.05$ as determined by ANOVA).
785 (C) NC and shRNA cells were infected with rSD16-MA virus for 12 h followed by
786 immunofluorescence detection of NP protein. All infections were at 2.0 MOI. Scale
787 bar = 15μm.

788

789 **FIG 12** FMRP is necessary for the replication of neurotropic H5N1 and H10N7 AIVs

790 in murine brain but not in lung. WT and FMRP$^{-/-}$ mice, in groups of 6, were infected
791 separately with neurotropic H5N1 and H10N7 virus at 10^6 EID_{50} of virus/mouse.
792 Virus isolation from brains (A) and lungs (B) of 3 mice was performed at 3 and 5 dpi.

793

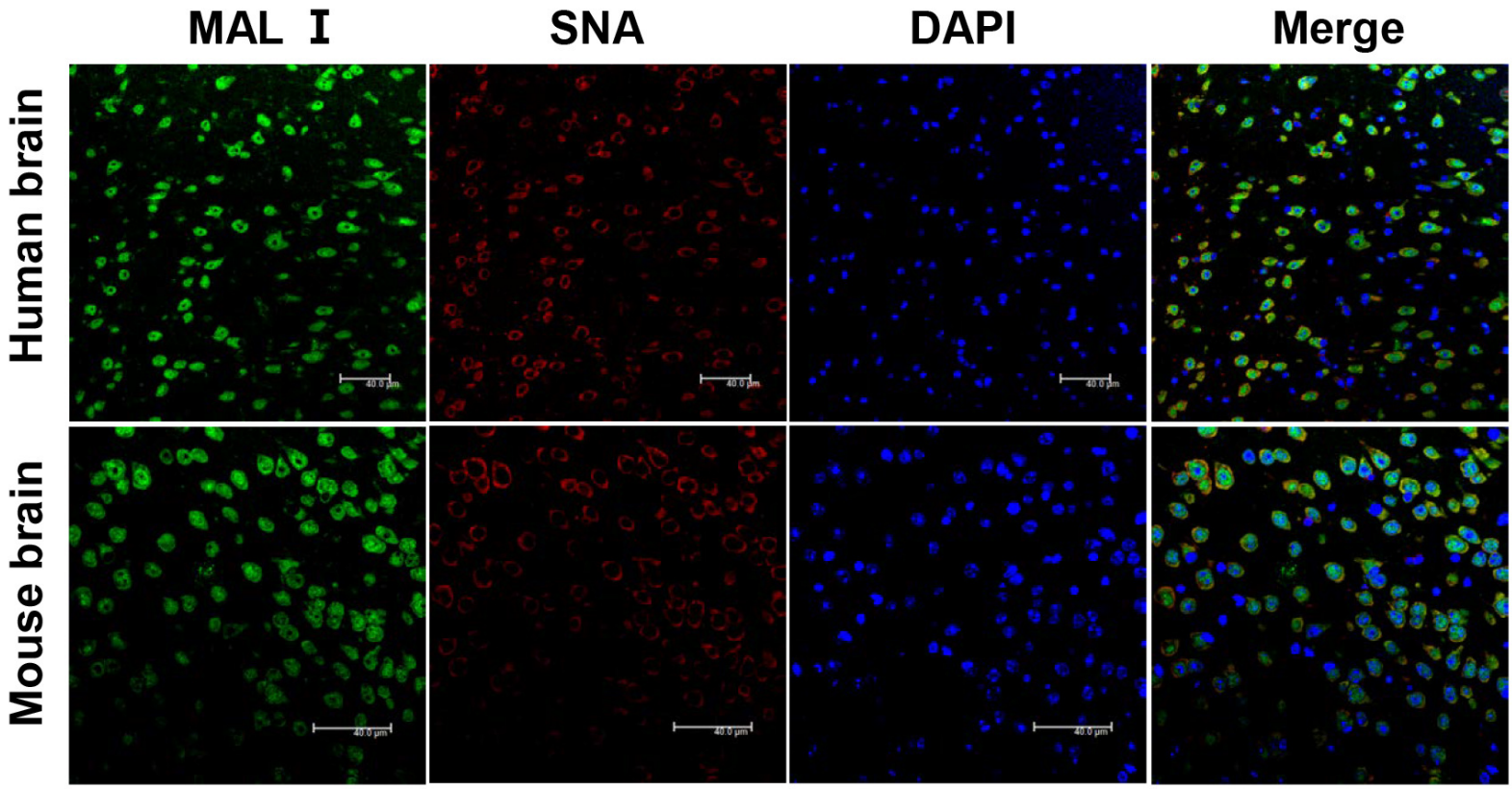
MAL I
SNA
DAPI
Merge
Human brain
Mouse brain

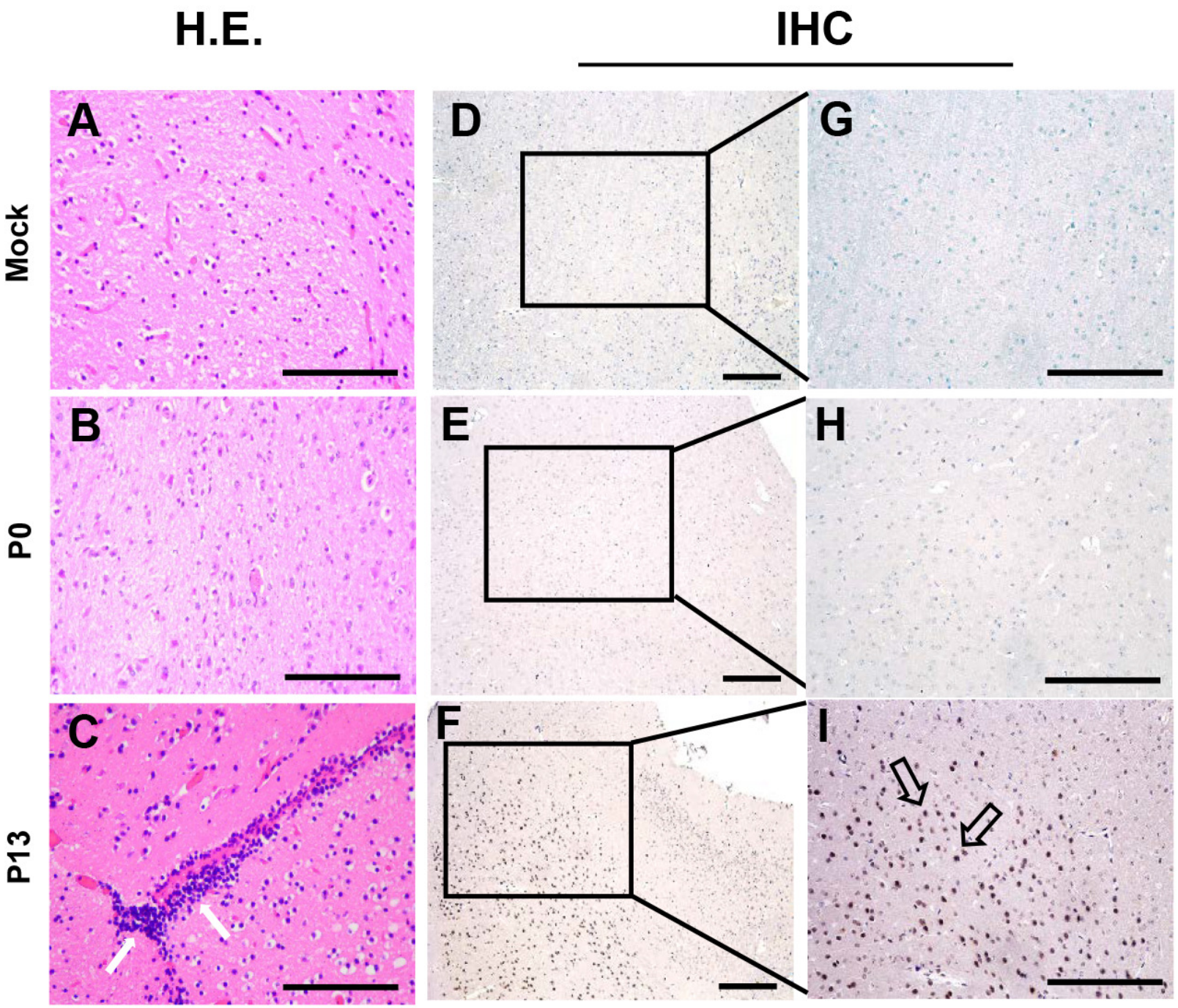
H.E.
IHC
Mock
P0
P13
A
B
C
D
E
F
G
H
I

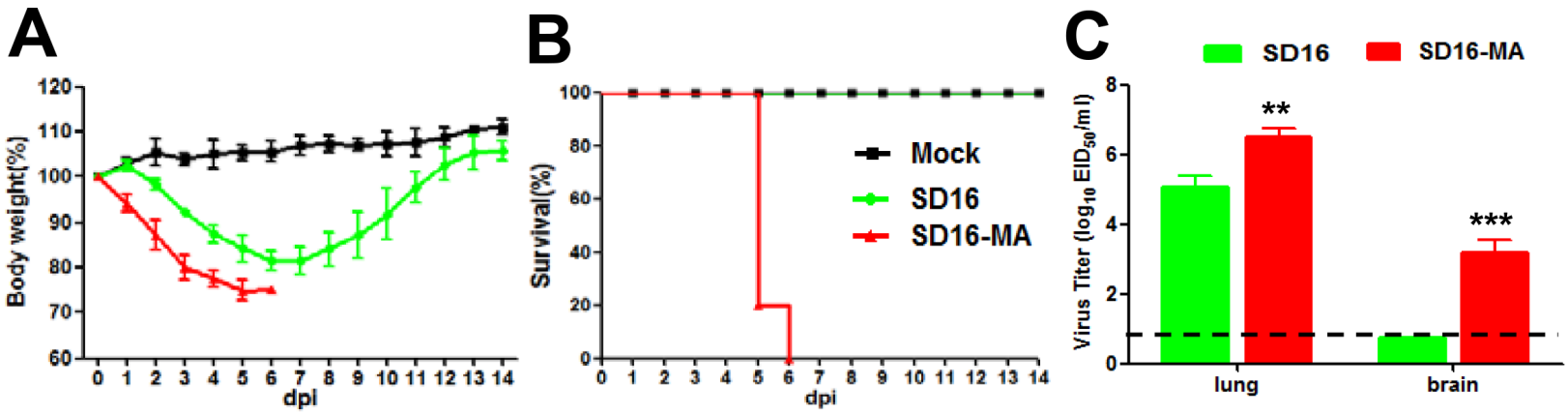
A
Body weight(%)
120
110
100
90
80
70
60
0 1 2 3 4 5 6 7 8 9 10 11 12 13 14
dpi
B
Survival(%)
100
80
60
40
20
0
0 1 2 3 4 5 6 7 8 9 10 11 12 13 14
dpi
Mock
SD16
SD16-MA
C
SD16
SD16-MA
Virus Titer (log10 EID50/ml)
8
6
4
2
0
**
***
lung
brain

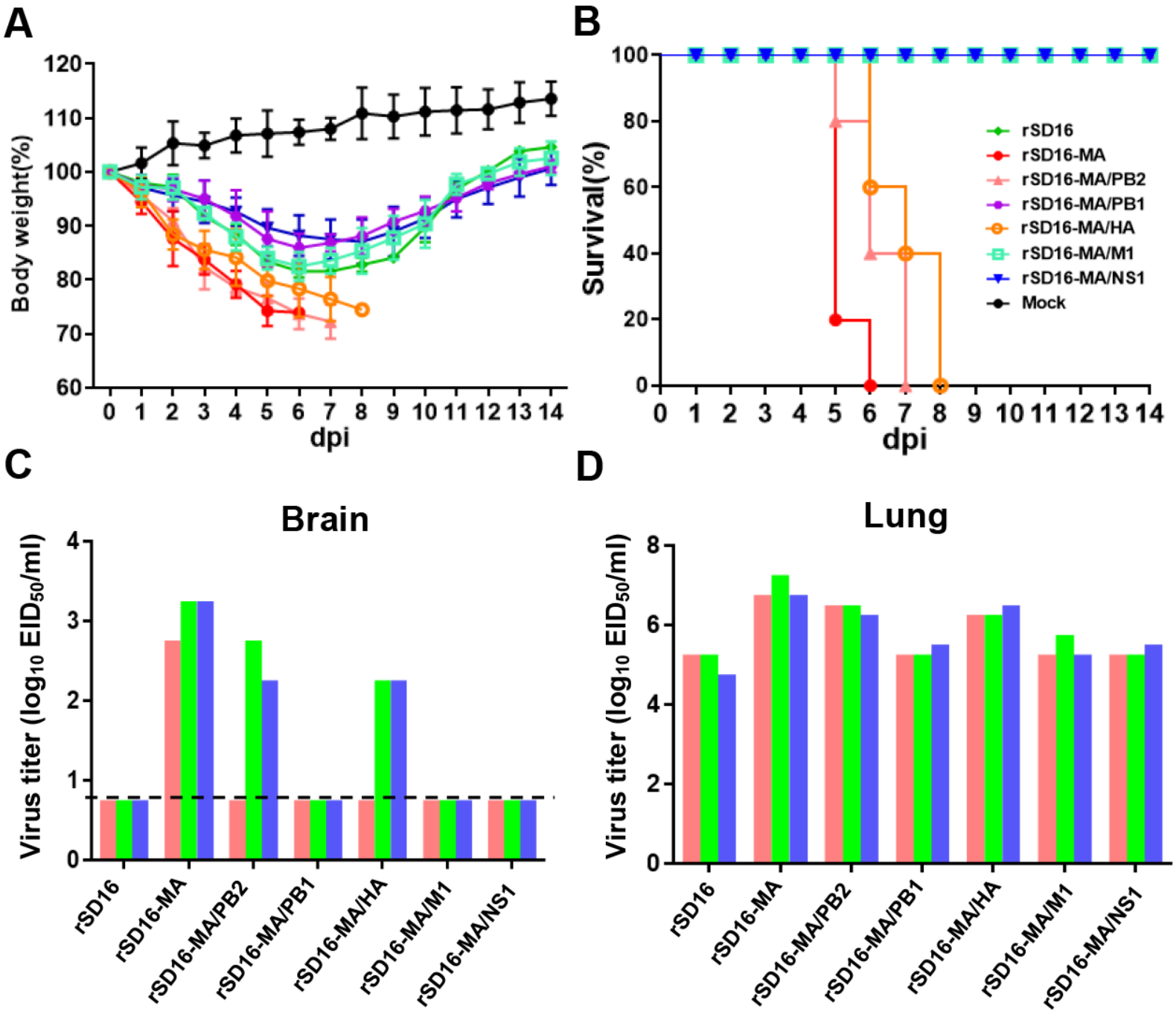
A
Body weight(%)
120
110
100
90
80
70
60
0 1 2 3 4 5 6 7 8 9 10 11 12 13 14
dpi
B
Survival(%)
100
80
60
40
20
0
0 1 2 3 4 5 6 7 8 9 10 11 12 13 14
dpi
rSD16
rSD16-MA
rSD16-MA/PB2
rSD16-MA/PB1
rSD16-MA/HA
rSD16-MA/M1
rSD16-MA/NS1
Mock
C
Brain
Virus titer (log10 EID50/ml)
4
3
2
1
0
rSD16
rSD16-MA
rSD16-MA/PB2
rSD16-MA/PB1
rSD16-MA/HA
rSD16-MA/M1
rSD16-MA/NS1
D
Lung
Virus titer (log10 EID50/ml)
8
6
4
2
0
rSD16
rSD16-MA
rSD16-MA/PB2
rSD16-MA/PB1
rSD16-MA/HA
rSD16-MA/M1
rSD16-MA/NS1

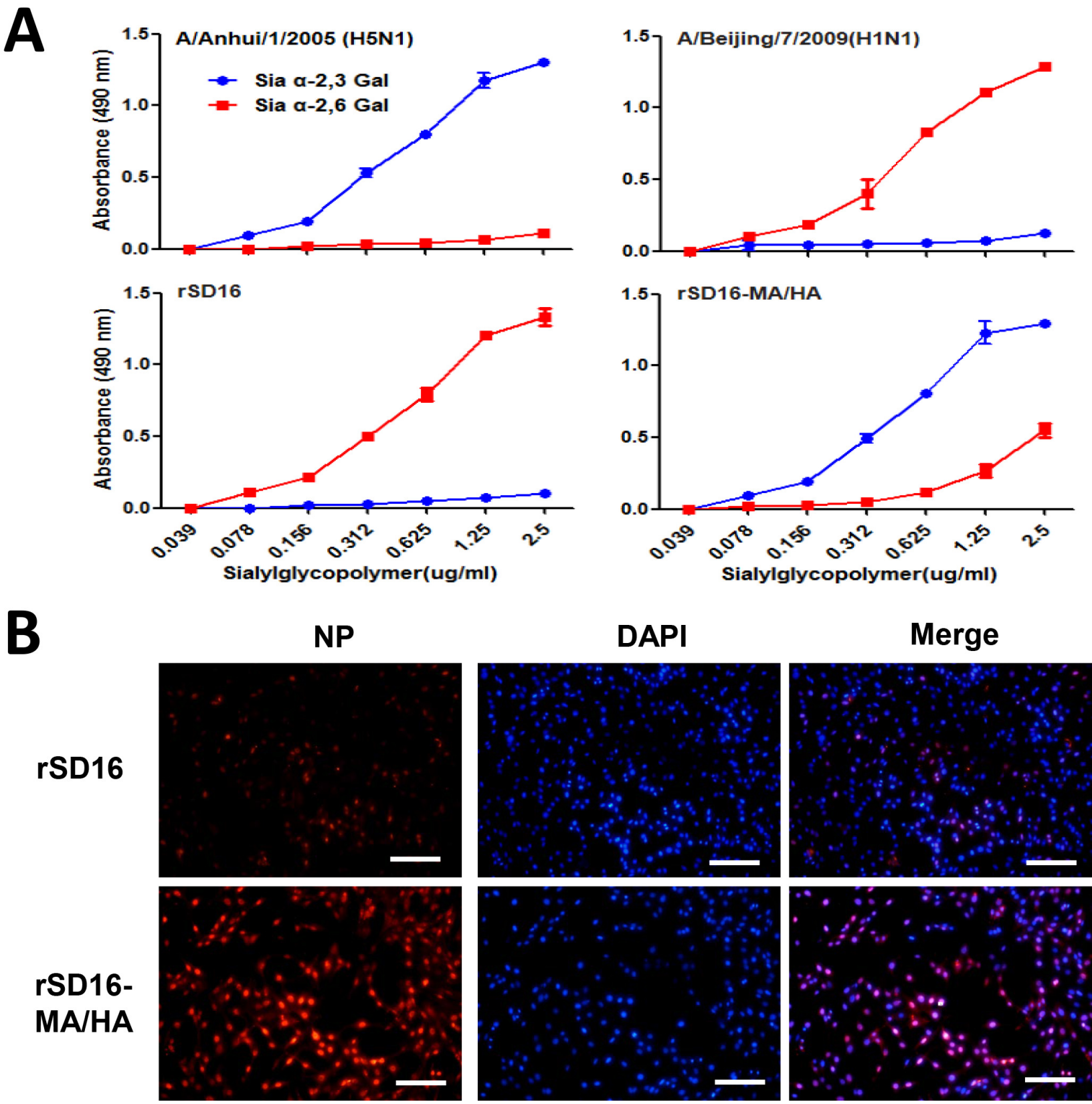
A
A/Anhui/1/2005 (H5N1)
Sia α-2,3 Gal
Sia α-2,6 Gal
A/Beijing/7/2009(H1N1)
rSD16
rSD16-MA/HA
Absorbance (490 nm)
1.5
1.0
0.5
0.0
0.039
0.078
0.156
0.312
0.625
1.25
2.5
Sialylglycopolymer(ug/ml)
B
NP
DAPI
Merge
rSD16
rSD16-
MA/HA

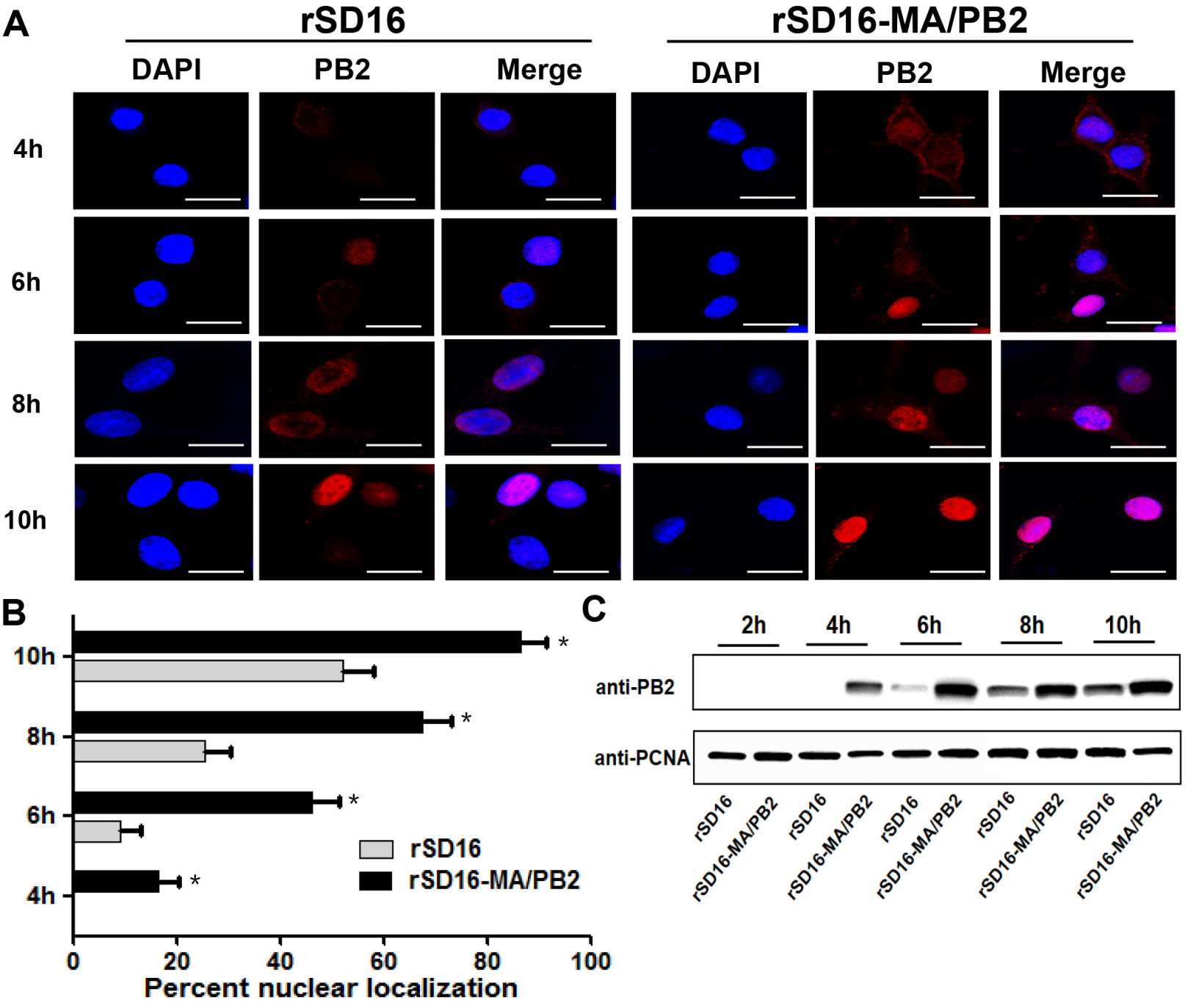
A
rSD16
rSD16-MA/PB2
DAPI
PB2
Merge
DAPI
PB2
Merge
4h
6h
8h
10h
B
10h
8h
6h
4h
*
*
*
*
rSD16
rSD16-MA/PB2
0
20
40
60
80
100
Percent nuclear localization
C
2h
4h
6h
8h
10h
anti-PB2
anti-PCNA
rSD16
rSD16-MA/PB2
rSD16
rSD16-MA/PB2
rSD16
rSD16-MA/PB2
rSD16
rSD16-MA/PB2
rSD16
rSD16-MA/PB2

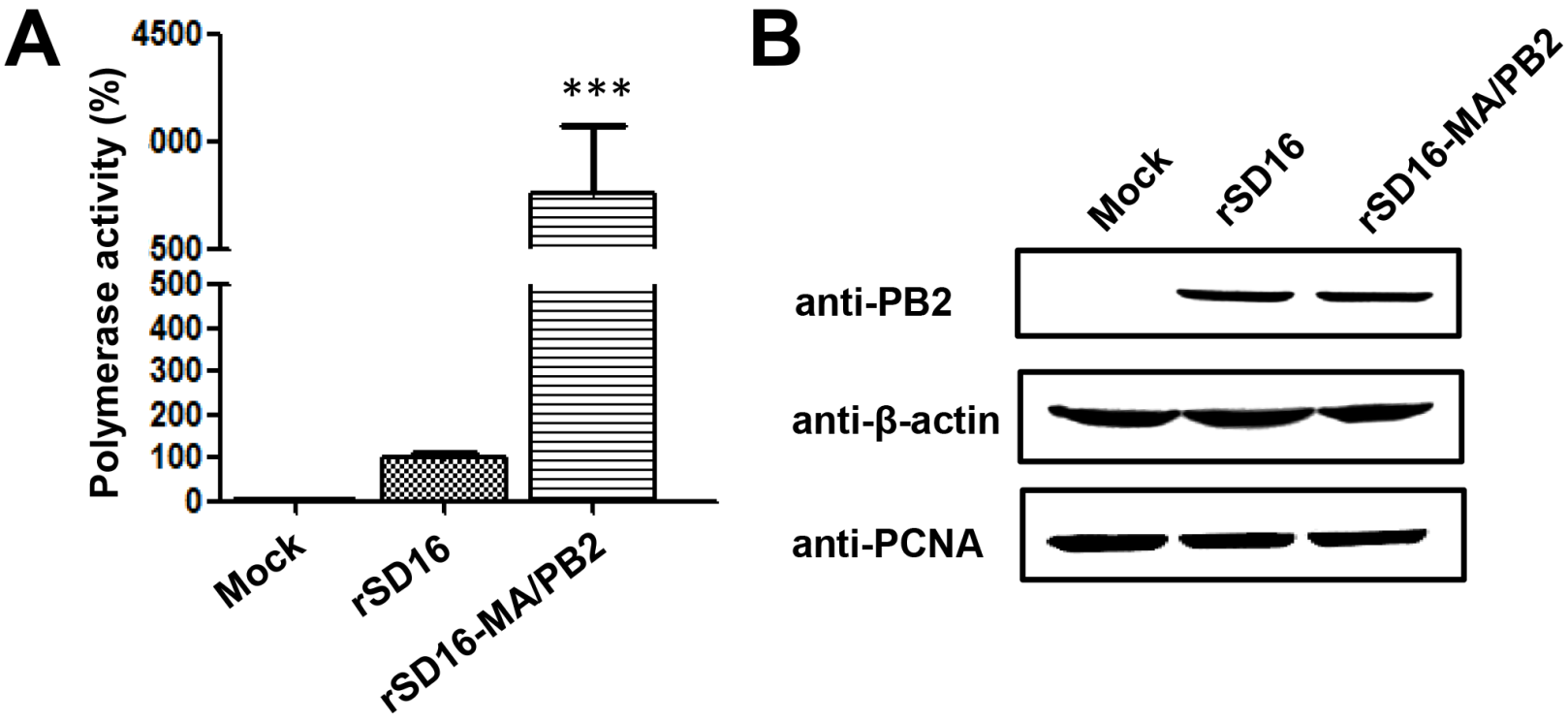
A
Polymerase activity (%)
4500
000
500
500
400
300
200
100
0
***
Mock
rSD16
rSD16-MA/PB2
B
Mock
rSD16
rSD16-MA/PB2
anti-PB2
anti-β-actin
anti-PCNA

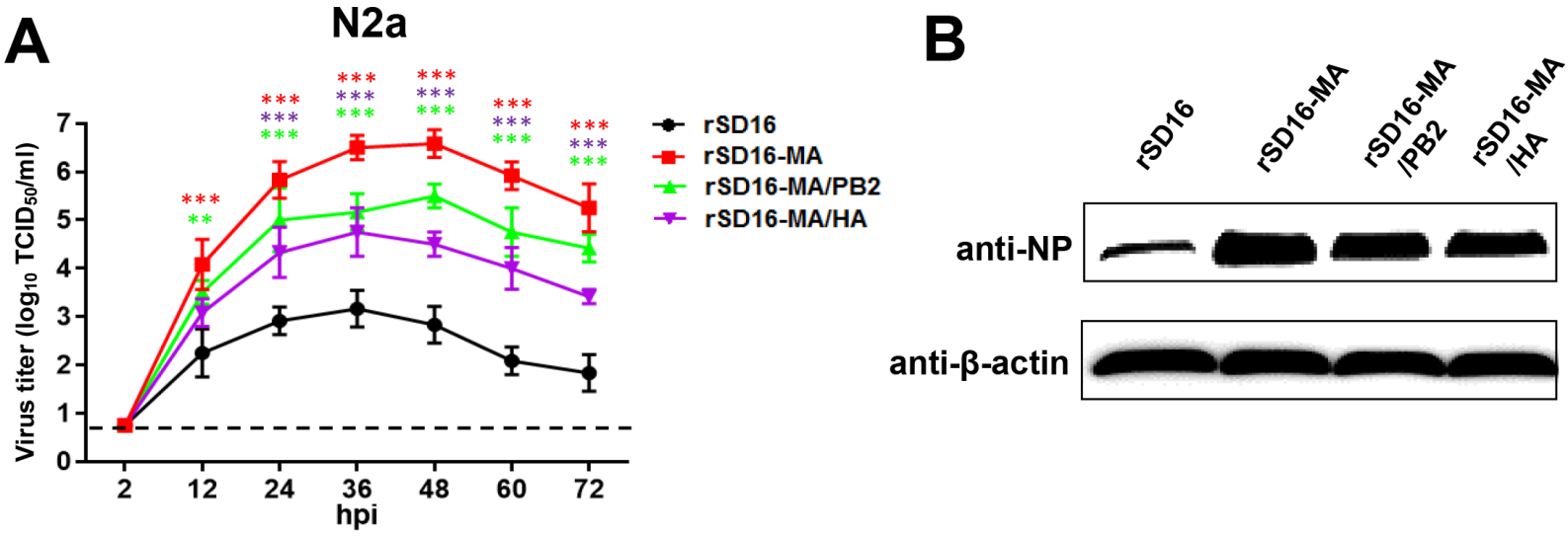
A
N2a
Virus titer (log10 TCID50/ml)
hpi
2
12
24
36
48
60
72
rSD16
rSD16-MA
rSD16-MA/PB2
rSD16-MA/HA
B
rSD16
rSD16-MA
rSD16-MA /PB2
rSD16-MA /HA
anti-NP
anti-β-actin

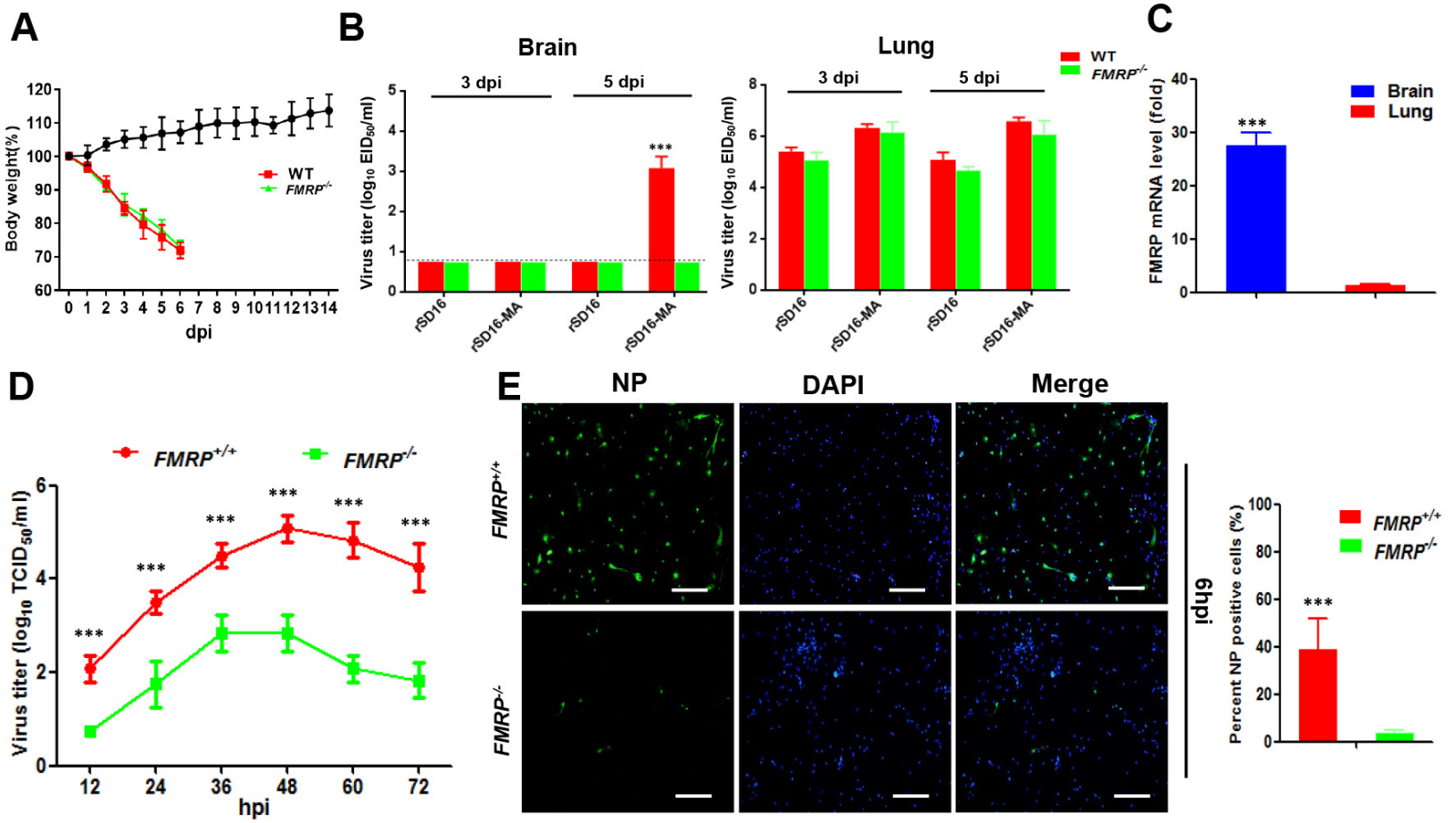
A
Body weight(%)
dpi
WT
FMRP-/-
B
Brain
Lung
3 dpi
5 dpi
Virus titer (log10 EID50/ml)
rSD16
rSD16-MA
C
FMRP mRNA level (fold)
Brain
Lung
D
FMRP+/+
FMRP-/-
Virus titer (log10 TCID50/ml)
hpi
E
NP
DAPI
Merge
6hpi
Percent NP positive cells (%)

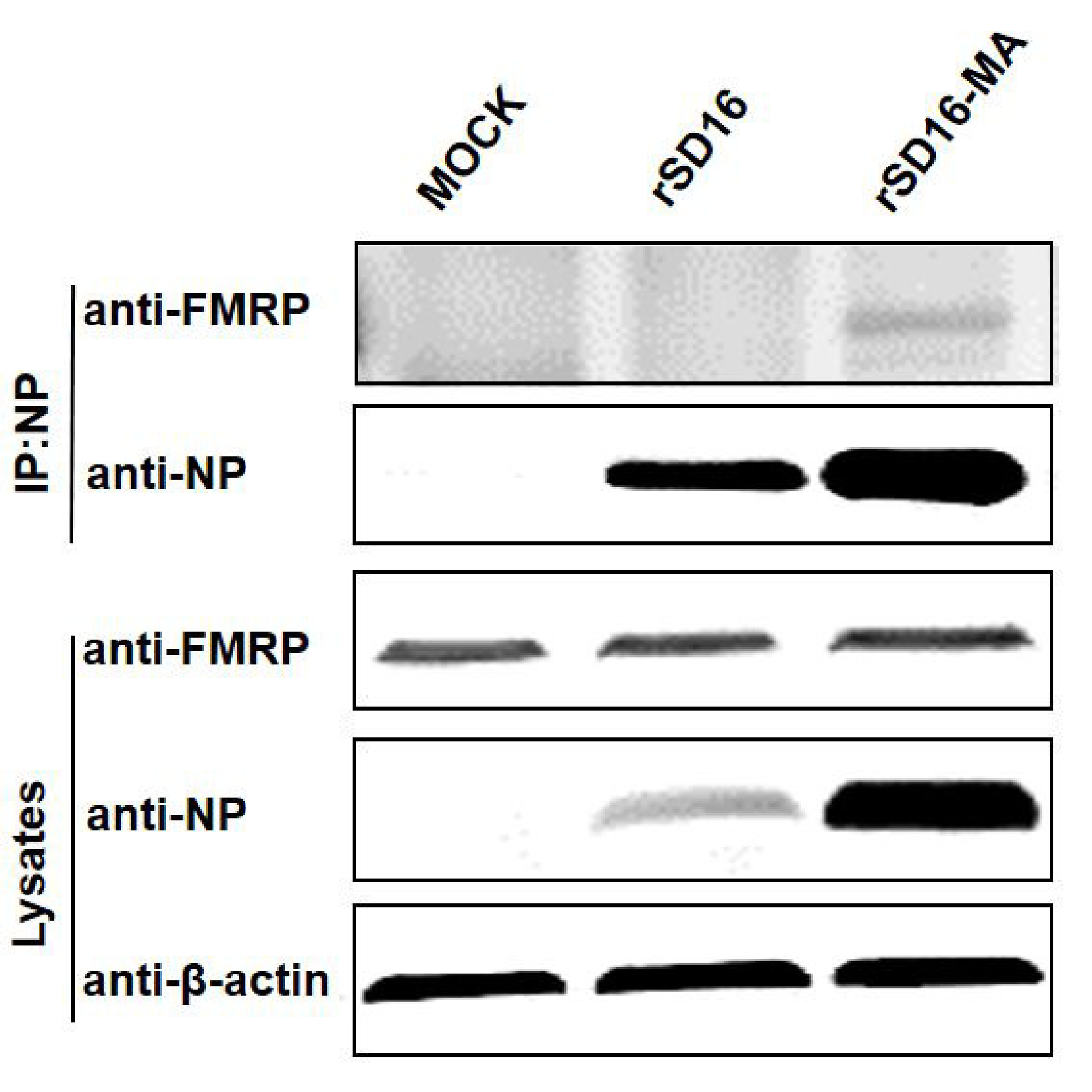
MOCK
rSD16
rSD16-MA
IP:NP
anti-FMRP
anti-NP
Lysates
anti-FMRP
anti-NP
anti-β-actin

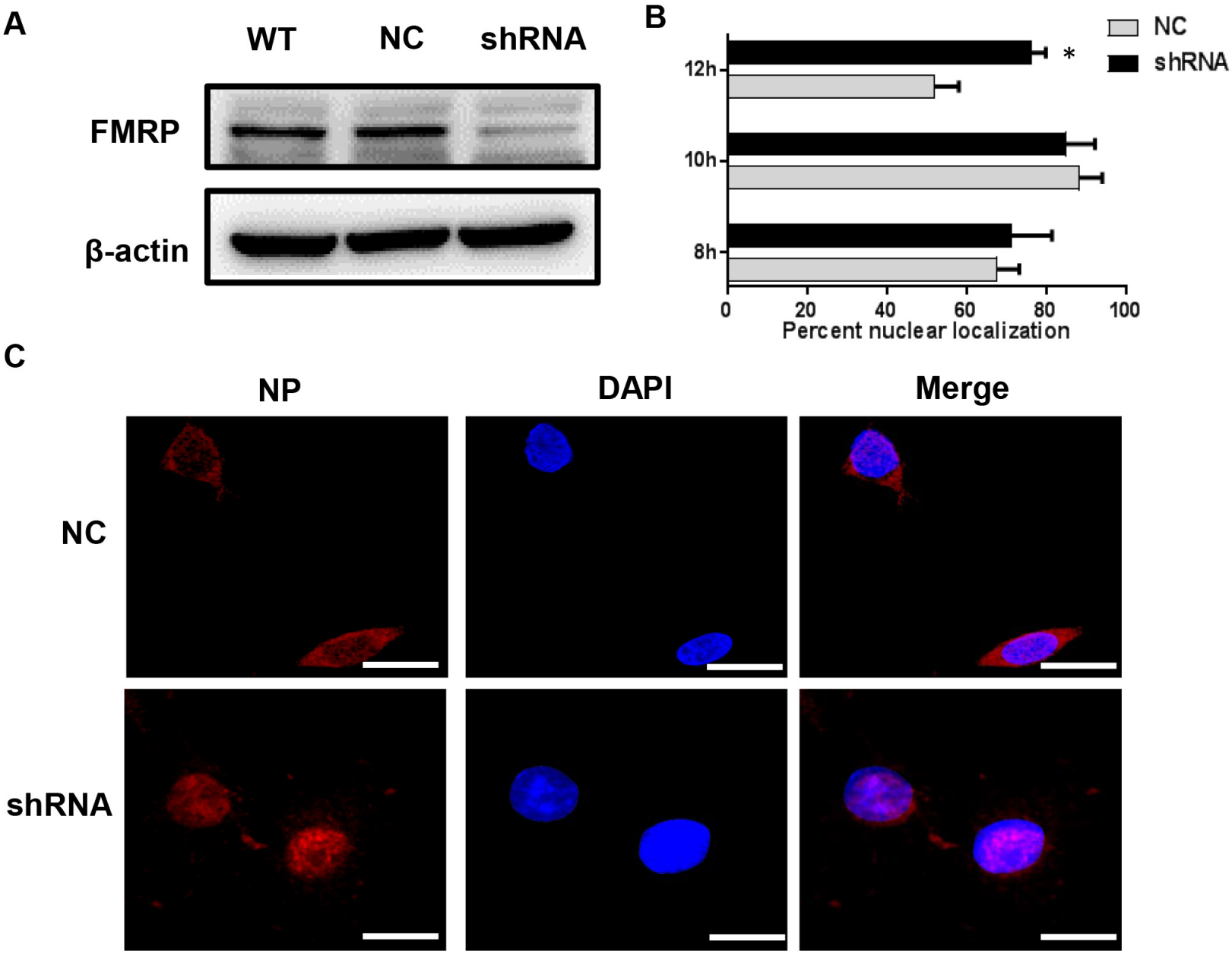
A
WT
NC
shRNA
FMRP
β-actin
B
NC
shRNA
12h
10h
8h
*
0
20
40
60
80
100
Percent nuclear localization
C
NP
DAPI
Merge
NC
shRNA

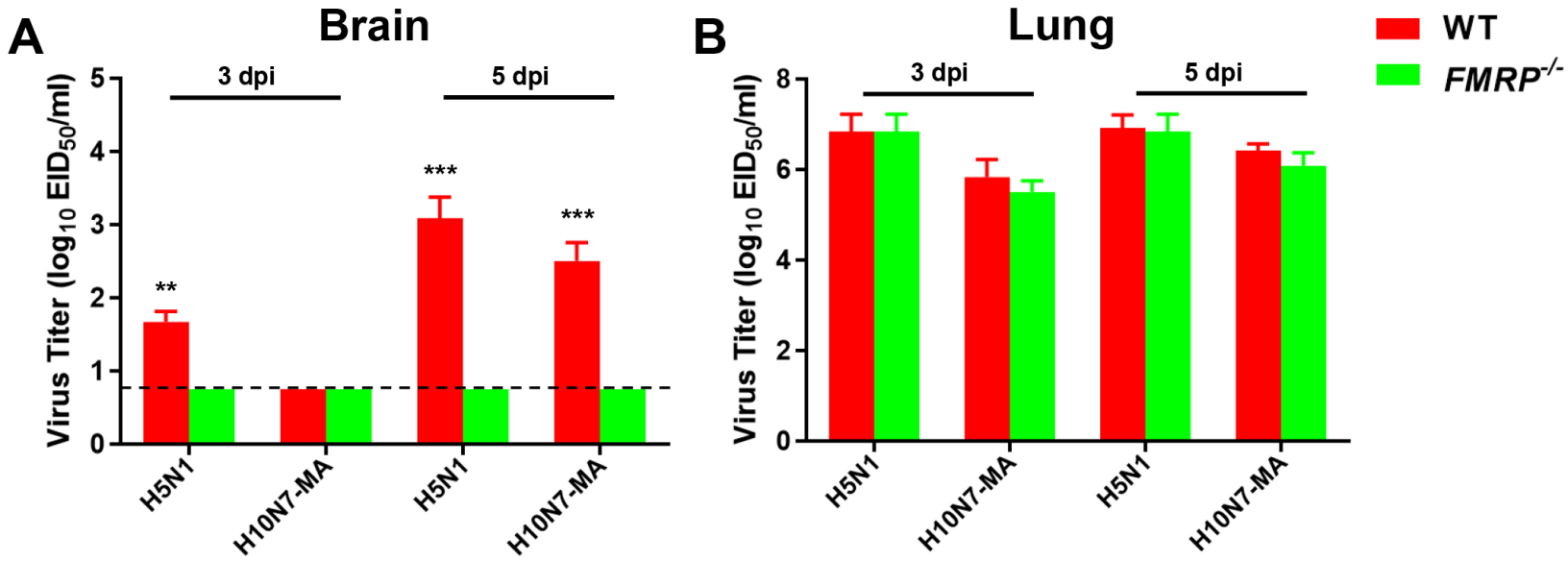
A
Brain
3 dpi
5 dpi
Virus Titer (log10 EID50/ml)
**
***
***
H5N1
H10N7-MA
H5N1
H10N7-MA
B
Lung
3 dpi
5 dpi
Virus Titer (log10 EID50/ml)
H5N1
H10N7-MA
H5N1
H10N7-MA
WT
FMRP-/-

TABLE 1 Amino acid substitutions of mutants isolated from mice.

Virus protein	Amino acid position	Presence of amino acid		Mutation frequency
		SD16	SD16-MA	
PB2	147	M	L	100% (30/30)
	250	V	G	100% (30/30)
	627	E	K	100% (30/30)
PB1	657	Y	H	100% (30/30)
	642	N	K	3% (1/30)
PA	129	I	T	3% (1/30)
	151	T	S	3% (1/30)
	588	S	P	3% (1/30)
HA	211	R	K	100% (30/30)
	226	L	Q	100% (30/30)
NA	204	S	T	20% (6/30)
M1	210	R	K	100% (30/30)
NS1	214	L	F	100% (30/30)